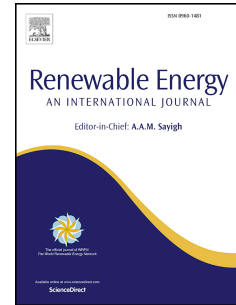


Journal Pre-proof

Soiling mapping through optical losses for Nigeria

Yusuf N. Chanchangi, Aritra Ghosh, Leonardo Micheli, Eduardo F. Fernández, Senthilarasu Sundaram, Tapas K. Mallick



PII: S0960-1481(22)01015-1

DOI: <https://doi.org/10.1016/j.renene.2022.07.019>

Reference: RENE 17376

To appear in: *Renewable Energy*

Received Date: 25 November 2021

Revised Date: 4 June 2022

Accepted Date: 4 July 2022

Please cite this article as: Chanchangi YN, Ghosh A, Micheli L, Fernández EF, Sundaram S, Mallick TK, Soiling mapping through optical losses for Nigeria, *Renewable Energy* (2022), doi: <https://doi.org/10.1016/j.renene.2022.07.019>.

This is a PDF file of an article that has undergone enhancements after acceptance, such as the addition of a cover page and metadata, and formatting for readability, but it is not yet the definitive version of record. This version will undergo additional copyediting, typesetting and review before it is published in its final form, but we are providing this version to give early visibility of the article. Please note that, during the production process, errors may be discovered which could affect the content, and all legal disclaimers that apply to the journal pertain.

© 2022 Published by Elsevier Ltd.

Soiling mapping through optical losses for Nigeria

Yusuf N. Chanchangi^{1*}, Aritra Ghosh¹, Leonardo Micheli², Eduardo F. Fernández³,
Senthilarasu Sundaram⁴, Tapas K. Mallick¹

¹Environment and Sustainability Institute (ESI), University of Exeter, Penryn Campus TR10 9FE, United Kingdom; ²Department of Astronautics, Electrical and Energetics Engineering (DIAEE), Sapienza University of Rome, Rome Italy; ³Advances in Photovoltaic Technology (AdPVTech), CEACTEMA, University of Jaén, 23071 Jaén, Spain; ⁴School of Engineering and The Built Environment, Edinburgh Napier University, Edinburgh, Scotland.

*Corresponding author: Yc486@exeter.ac.uk

Title: Dr

Name: Yusuf N. Chanchangi,

Affiliation: ¹Environment and Sustainability Institute (ESI), University of Exeter, Penryn Campus TR10 9FE, United Kingdom

Email: yc486@exeter.ac.uk

All Authors:

Title: Dr

Name: Yusuf N. Chanchangi,

Affiliation: ¹Environment and Sustainability Institute (ESI), University of Exeter, Penryn Campus TR10 9FE, United Kingdom:

Email: yc486@exeter.ac.uk

Title: Dr

Name: Aritra Ghosh,

Affiliation: ¹Environment and Sustainability Institute (ESI), University of Exeter, Penryn Campus TR10 9FE, United Kingdom

Email: A.Ghosh@exeter.ac.uk

Title: Assistant Professor

Name: Leonardo Micheli,

Affiliation: Department of Astronautical, Electrical and Energy Engineering (DIAEE), Sapienza University of Rome, Rome 00184, Italy.

Email: leonardo.micheli@uniroma1.it

Title: Associate Professor

Affiliation: Associate Professor

Name: Eduardo F. Fernández

Affiliation: eduardo.fernandez@ujaen.es

Title: Associate Professor

Name: Senthilarasu Sundaram

Affiliation: School of Engineering and The Built Environment, Edinburgh Napier University, Edinburgh, Scotland.

Email: S.Sundaram@napier.ac.uk

Title: Professor

Name: Tapas K. Mallick

Affiliation: ¹Environment and Sustainability Institute (ESI), University of Exeter, Penryn Campus TR10 9FE, United Kingdom

Email: T.K.Mallick@exeter.ac.uk

Soiling mapping through optical losses for Nigeria

Yusuf N. Chanchangi*, Aritra Ghosh, Leonardo Micheli, Eduardo F. Fernández,
Senthilarasu Sundaram, and Tapas K. Mallick

¹Environment and Sustainability Institute (ESI), University of Exeter, Penryn Campus TR10 9FE, United Kingdom. ²Advances in Photovoltaic Technology (AdPVTech), CEACTEMA, University of Jaén, 23071 Jaén, Spain.

*Corresponding author: yc486@exeter.ac.uk

Abstract

Soiling consists of the accumulation of dust on the solar panel's surface and has a deleterious effect on solar photovoltaic devices' performance, which varies with location. However, soiling losses and rates are significantly under-reported or underestimated since regional differences and seasonal variations are overlooked. Accurate prediction of PV soiling losses for a particular location can save revenue losses associated with a solar PV system. This research investigated the effect of soiling on PV performance through optical losses by employing a low-cost soiling station. Low iron glass coupons (5 mm x 5 mm) were exposed on three angles (vertical, tilt-45°, and horizontal) in seven sites across Nigeria to collect annual, seasonal and monthly soiling data. Each coupon was then subjected to optical characterisation using a spectrometer and imaging analysis using the SEM/EDX. The finding shows significant optical losses across the country, with all the highest rates recorded on coupons exposed on the horizontal plane, where the maximum loss of 88% was recorded on the Abuja, North Central (ABV) coupon. SEM/EDX finding illustrated minerals with the potential to affect light transmittance, and the pollutant data confirmed the particles. The optical results were further employed to map the soiling distribution across the country. A wide deviation was observed from the data on the Global Solar Atlas, as it disproportionately underestimated the soiling losses across the world.

Keywords: Optical losses; PV soiling; Mapping; Dust Particles; Nigeria

Nomenclature	
$S(\lambda)$	Relative spectral distribution of solar radiation
$T(\lambda)$	Spectral transmittance
$\Delta\lambda$	Change in wavelength
P_{out}	Power output
τ_{clean}	Transmittance data of clean coupon
τ_x	Transmittance data of an exposed coupon on an unknown angle
$\Delta\tau_x$	Change of transmittance data of an exposed coupon on an unknown angle
$\Delta\tau_{(Optimum)}$	Calculated change of transmittance of a coupon at an optimum angle
$\beta(x)$	The optimum tilt angle of a particular station
$\beta_{(0)}$	Horizontal plane (angle 0°)
$\beta_{(45)}$	The tilt angle of 45°
$\Delta\tau_{(0)}$	Soiling losses recorded on a coupon positioned on a horizontal plane
$\Delta\tau_{(45)}$	Soiling losses recorded on a coupon positioned at angle 45°
Z_K^*	The smooth estimate produced by Kriging interpolation
λ_i	Weight for Z_i
Z_i	Variable
Z_V	Actual value
$\bar{C}(V, V)$	Covariance between the variables of the samples
μ	Lagrange parameter
$\bar{C}(v_i, V)$	Covariance between the estimations and the variables of the samples
CO	Carbon Monoxide
O ₃	Ozone

NO ₂	Nitrogen oxide	28
SO ₂	Sulphuric oxide	29
PM ₁₀	Particulate Matter 10 micrometres and smaller	30
PM _{2.5}	Particulate Matter 2.5 micrometres and smaller	31
		32
		33

34

Units		35
µg/m ³	Microgram/meter cube	36
kWp	kiloWatt peak	37
MW	MegaWatt	38
mm	millimetre	39
		40
		41
		42
		43

44

Abbreviation		
3D	3 Dimension	
ABS	Acrylonitrile Butadiene Styrene	
ABV	Abuja	
AQI	Air Quality Index	
BSE	Back Scattered Electron	
EDX	Energy Dispersive X-ray	
ENU	Enugu	
ESMAP	Energy Sector Management Assistance Program	
GIS	Geographical Information System	
GSA	Global Solar Atlas	
GW	Giga Watt	
IEA	International Energy Agency	
KAD	Kaduna	
LOS	Lagos	
MENA	The Middle East and North Africa	
MIU	Maiduguri	
NIR	Near Infra-Red	
PHC	Port Harcourt	
PV	Photovoltaic	
RE	Renewable Energy	
SE	Secondary Electron	
SEM	Scanning Electron Microscope	
SMS	Small-Medium Scale	
SOK	Sokoto	
UV	Ultra-Violet	
VIS	Visual	
WHO	World Health Organization	

45

46 1 Introduction

47 Solar photovoltaic (PV) is rapidly penetrating the global energy market, having an annual additional
 48 capacity of about 115 GW and a total capacity of 627 GW in 2019 [1]. However, the technology faces
 49 environmental challenges such as soiling, which has a detrimental effect on its performance, as reported
 50 in a number of publications [2-5]. Soiling is a factor that can degrade the performance of PV by reducing
 51 the amount of incident transmitted light upon solar cells. The losses due to soiling vary with location,
 52 human activities in the region, PV systems' design, angular position, mounting orientation, surface
 53 covering material, and climate [6, 7]. The reported soiling loss rates range from as low as 0.5% reduction
 54 of PV output in a day [8], 63% in a month [9], to about 50% reduction of PV yield in 6 months[10]

55 without cleaning. A clean low iron glass has 91% transparency [11], reducing the amount of irradiance
56 reaching the solar cells and preventing them from generating optimum yield. Since the most commonly
57 used and one of the best PV covering materials available in the market already possesses some
58 transmittance limitations, there is a need to prevent or reduce any further optical losses to ensure that
59 maximum irradiance reaches the solar cell to harvest higher yield. As stated earlier, the soiling loss rates
60 cannot be constant for different regions since they vary with the location, depending on the human
61 activities and the climate. Some research works reporting loss variation in various regions are provided
62 in the supplementary material.

63
64 Employing a constant value as a soiling loss cannot be accepted as it would illustrate an unrealistic PV
65 potential of a region. Standards assume fixed soiling loss values, such as $\pm 5\%$ in the AS4509.2 (3.4.3.6)
66 [12], 2% and 3% in SAND2014-19199 [13], and 3% in Enphase Energy [14], which might be grossly
67 inappropriate for some regions. Tanesab et al. [15] recommended reviewing soiling rates and
68 considering regions with high solar energy potential and extreme weather conditions. In addition, the
69 Global Solar Atlas (GSA) [16] used constant soiling loss values for categories of installation, such as;
70 3.5% for 1kWp, 4.5% for small residential, 4% for medium commercial, 3.5% for large scale, and 6%
71 of floating large scale. However, GSA [16] clearly stated that the PV yield they provide is an estimation
72 value as some important factors (such as soiling) are not adequately calculated. The Global solar atlas
73 (GSA) is a platform that provides solar energy resources across the globe; which SolarGIS and finance
74 were developed by the Energy Sector Management Assistance Program (ESMAP) through the World
75 Bank fund. The GSA provided solar information like no other; it is the best platform available so far
76 that provided introductory-level data that could help researchers, policymakers, and PV companies
77 decide. These values grossly underestimate the magnitude of PV yield degradation that soiling losses
78 could cause in some regions across the world, especially the Middle East and North Africa (MENA),
79 Saharan, sub-Saharan Africa, and regions with high dust atmospheric dust.

80
81 Li et al. [17] investigated the soiling on fixed, one-axis tracking (OAT) and two-axis tracking (TAT)
82 modules employing modelling techniques to develop a map using 12 years of particulate matter, global
83 solar irradiance, and precipitation data. The study reported a more than 50% PV yield reduction for
84 heavily polluted areas such as the Middle East, Africa, and China. However, this study ignored a crucial
85 factor (such as wind) that can significantly influence deposition when its velocity is low and acts as
86 natural cleaning when its speed is high, thereby overestimating deposition rate/accumulation and
87 underestimating natural removal rate [18-21]. The study does not provide details on the soiling losses
88 in Western, Central, and Eastern Africa, subject to substantial dust generation levels due to their
89 geographical terrain, human activities and proximity to the largest global dust generation region, the
90 Sahara desert.

91
92 Mithu et al. [22] developed a soiling map to illustrate the global PV soiling and predict revenue loss
93 considering regional optimal cleaning frequency using reported experimental data of 132 sites from
94 literature. Their finding shows that Asia has the highest soiling rate of 1%–2%/day, followed by the
95 Middle East with 0.7%–1.5%/day, mid-Africa (between 0 and 15°N latitudes) with 0.5%–1%/day and
96 the rest of the world mostly below 0.5%/day. They predicted a global revenue loss for the optimal
97 cleaning cycle to be around 1%–5.5%. Modelling global data using 132 sites from reported
98 experimental results that might have become obsolete to develop a global map could vastly
99 underestimate and underreport the value of some regions, such as West Africa and Central Africa, where
100 only two reported values were used for the entire map.

101
102 Micheli et al. [23] developed a regional soiling map by employing five spatial-interpolation approaches
103 extracted from PV performance and soiling station data to estimate nearby sites in the United States of
104 America (USA). Their findings show that an average soiling ratio could be estimated with a root-mean-
105 square error (RMSE) of 1.4% and coefficients of determination of about 74%. Their analysis shows that
106 the error could be reduced to 1.1% when soiling sensors are deployed to determine the soiling rate
107 compared to estimation, with about 78% determination coefficient variation between determined and
108 estimation values. Their findings show that deploying sensors will reduce errors, especially when the
109 distance between sites is reduced to below 50 km. Although the study used soiling station and PV
110 performance data from 83 sites across the United States and laid a foundation for this kind of study, the

111 study ignored weather parameters related to soiling and other influences such as temperature and
112 cabling losses, shading losses and other parameters.

113
114 Cordero et al. [24] reported the effect of soiling on PV performance, where findings were illustrated in
115 a map. The study was conducted in five sites around the Atacama desert, which transect approximately
116 1300 km from latitude 18° S to latitude 30° S. Four PV modules were deployed where to are cleaned,
117 and the others were left to accumulate dust. The finding shows a 39% (in Arica, a city around the
118 Atacama desert) annual PV yield reduction in the northern region and 3% or less in the southern part
119 (Copiapo, La Serena, and Calama). Although a good study was provided, the following flaw has cast
120 doubt on the findings: the study ignored the effect of temperature when calculating soiling losses based
121 on the disparity of PV yield. There are so many irregularities in cleaning approaches as high personnel
122 rotation was involved, where each cleaner uses a different cleaning pattern. The research highlighted
123 significant uncertainty due to a weaker correlation between AOD and the soiling rate. The experiment
124 ignored the influence of tilt angle and exposed module on a fixed angle based on a site's latitude, and
125 previous studies [25, 26] reported a 10% variation caused by the influence of angular positioning. The
126 soiling rate data presented was not spatially distributed; instead, a distinct value was illustrated for the
127 region, with no interpolation estimates for various sites. The monthly soiling losses variation was
128 calculated using the same results, which could lead to estimation errors of PV yield in the findings [25,
129 26] published.

130
131 Tanaka and Chiba [27] reported that Northern and West Africa are the regions with the most significant
132 atmospheric dust loading rate across the globe, and Nigeria happens to be one of the regions. As
133 previously mentioned, an enormous amount of work has been carried out in the field of soiling on PV,
134 but this region (Nigeria) has received significantly less attention in recent years. However, some areas
135 with high solar energy potential, low PV penetration and high energy deficiency (a wide gap between
136 demand and supply), such as Nigeria, are still far behind in meeting up the sustainable development
137 goal 7 (affordable, reliable and clean energy for all). The World Bank [28] highlighted a massive energy
138 deficit where it was showing that Nigeria will have a population of 206 million in 2020, with only about
139 60% having access to energy that is unreliable and unsteady. The International Energy Agency (IEA)
140 [29] stated that Nigeria's Renewable Energy (RE) target is 30 GW with 5.3 GW solar mini-grid and 2.8
141 GW small, medium scale (SMS) by 2030, but less than 10 MW PV installation was recorded in 2020.

142
143 Despite the reports presented above, it is notable that only a few studies [23, 30] considered multiple
144 sites for data collection in their research. The literature showed results variation from studies conducted
145 in the same region, which supports the claim that dust accumulation is location-dependent and the
146 soiling rate of each region varies and should therefore be determined. In addition, when conducting an
147 extensive literature review, it was observed that most soiling losses were recorded in a single location,
148 during a particular season or few weeks-months, while ignoring seasonality and more extended
149 exposure duration variation makes it extremely difficult to know the soiling rate of a country or region.
150 It was also observed that some of these studies position coupons or PV modules on a single angle,
151 limiting their analysis and prediction level. Similarly, it was observed that disregarding influencing
152 factors could lead to inaccuracy of estimations. There has been an increased recognition that more
153 attention is needed to be put on PV soiling in various regions with high solar energy potential and less
154 PV penetration to scale up the application of renewable energy (RE) technology and reduce the gas
155 emission that promotes climate change. Therefore, deploying multiple sensors or installing soiling
156 stations over a more extended period could acquire temporal soiling variations and spatial data to
157 provide more accurate estimations.

158
159 Nigeria is a strategic region with a high energy deficit and substantial solar energy potential, but its
160 proximity to the source of Saharan dust is a concern to the performance of PV technology when
161 deployed [2]. This study investigated the effect of soiling on PV performance, focusing on
162 environmental variability as an influencing factor through developing a very simple, low-cost soiling
163 station that collects optical losses data to generate a PV soiling losses map without installing a
164 photovoltaic system. The concept provided is not only limited to the region of study; it could be
165 replicated elsewhere and could also be used for large scale PV soiling predictions in the region,
166 elsewhere, or in global scenarios. Different locations and their relative angular soiling losses are

167 investigated to accommodate other PV installation applications such as BIPV (Building Integrated PV),
168 VIPV (Vehicle Integrated PV), and exterior/interior decorations operating on varying angular axes. The
169 data provided could be used as a tool to help mitigate soiling effects on new PV installations in Nigeria.
170 Indeed, it can be used to estimate the impact of soiling and optimise the operations and maintenance
171 cycles even before PV plants are operational. The information provided in this report is not only limited
172 to the solar energy industry but could entice potential readers and citations from the glass, financial,
173 chemical, mechanical and mining industries. The soiling map is compared with a map published on the
174 GSA website for validation, presenting variations. The study's secondary objectives are to examine the
175 accumulated dust samples through elementology and mineralogy studies to identify their minerals,
176 including each diaphaneity. The morphological characterisation was also conducted to categorise the
177 regional depositions on the coupons, which was correlated with the air quality index (AQI). Optical
178 losses and weather parameters were correlated for analysis purposes to determine the cause of
179 accumulation on coupons and seasonality with significant concerns.

181 **2 Method**

182 Soiling in Nigeria was investigated using low iron glass coupons across geopolitical zones in the
183 country. A simple in-house low-cost research jig was designed using solid works and fabricated with a
184 3D printer (Stratasys uPrint SE 3D printer) using an ABS (Acrylonitrile Butadiene Styrene) P430XL
185 material. This research jig was selected after an initial comparative durability test using ABS, polylactic
186 acid (PLA), wooden, and metallic material since it was intended to be exposed under harsh
187 environmental conditions. Results show a high chance of particles moving onto the surfaces of coupons
188 from wood and rusted metal during extreme weather conditions, while the PLA failed and bent when
189 left in hot water (60°) over the period of two days. The ABS material has excellent thermal
190 characteristics and remains stable at temperatures between -20° to 80°C. The same material was used
191 to produce the transportation crates that reduce the shaking of coupons that could cause the removal of
192 accumulated dust from coupons' surfaces and prevent sample breakage. Each crate was examined after
193 transport to check if the particles were removed from the coupon during transport, but surprisingly the
194 majority of the crates were found to be clean, and the unclean ones could not substantiate any findings.

195
196 About 315 pieces of 50 mm x 50 mm x 4 mm coupons of low iron glasses were distributed in the six
197 geopolitical zones (North-Central, North East, Northwest, South East, South-south (Niger-Delta), and
198 South-West) and the main base of data collection (Kaduna). A more detailed description and
199 illustrations of the sites, set-up, transportation crates, installation, and sketches are presented in Fig. 1.
200 Each station has three holders (one for monthly, one for seasonal and one for annual coupons), and each
201 holder has three slots (one for vertical, one for tilt and one for horizontal) for exposing coupons to
202 outdoor weather conditions. Angular optical soiling was investigated in this study to provide losses data
203 consideration positioning variation that could be used for correction when PV technologies are deployed
204 for various applications such as BIPV (Building Integrated PV), BAPV (Building attached/applied PV),
205 VIPV (Vehicle integrated PV), solar farms (large grid), isolated solar micro, and mini-grid, car parking
206 roofing and interior decoration. Some of these applications allow the positioning of PV absorbing
207 surfaces at a location-specific optimum angle, while others do not allow it due to their kind of
208 application. In addition, some PV assets are sometimes deployed with solar single/dual-axis tracking
209 technology that makes it follow the sun throughout the day, making the technology encounter dust
210 accumulation at varying angular positions. The angular optical losses data could provide estimations
211 that could be used for maintenance planning.

212
213 The distribution of coupons in various locations across the country is shown in Fig. 1 Table 2. Soiling
214 stations with coordinates, fixed optimum angular PV positioning with the recorded Mineral and their
215 transparency characteristics, and the AQI/PM data obtained from Air Plum Lab. Monthly coupons are
216 exposed on the first day of the month, and then the coupon will be removed and replaced with a new
217 clean coupon on the first day of the following month. Seasonal coupons were installed at the beginning
218 of September when the research started to assume the wet season was coming to an end and marked the
219 dry season's outset. Seasonal coupons were removed and replaced according to specific locations'
220 seasons. Annual coupons were exposed at the end of the year and allowed to last for 12 calendar months
221 before they were removed. All exposed coupons were sealed in special crates fabricated using the

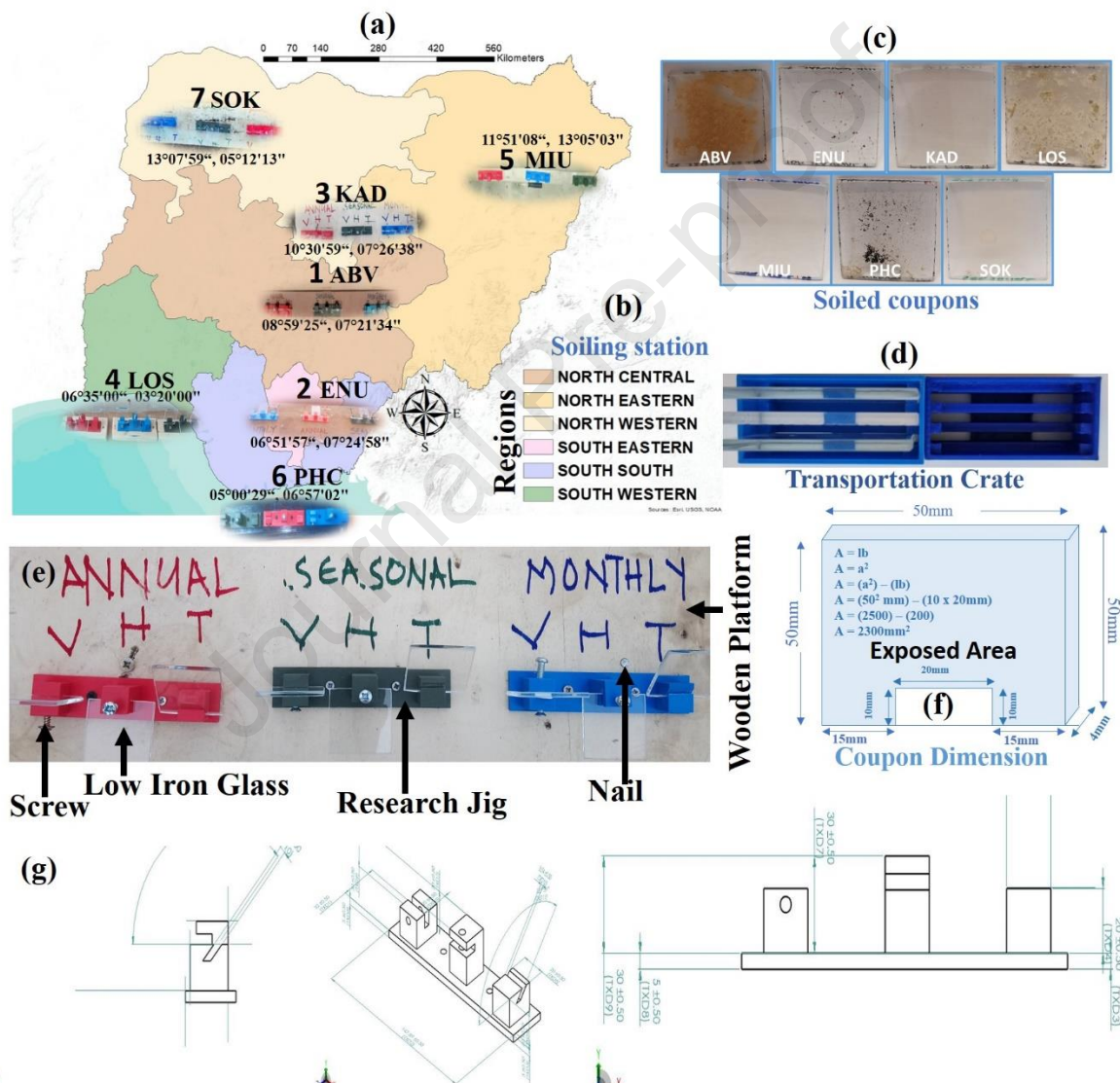
222 above-mentioned 3D printer and transported back to the solar laboratory at the University of Exeter for
 223 detailed characterisation.

224

225 Table 1: Coupons dimension and distribution across all stations

Coupons (Low Iron Glass)			Coupons: 3 (Vertical, Horizontal and Tilt) Seasons: 2 (Dry and Raining) Sites: 6 Geopolitical Zones and main base (see Fig. 1)
Length	50 mm		
Height	50 mm		
Thickness	4 mm		
Monthly	3 coupons x 7 sites x 12 months	252	
Seasonal	3 coupons x 7 sites x 2 seasons	42	
Annual	3 coupons x 7 sites x 1 year	21	
TOTAL		315	

226



227

228 Fig. 1. Soiling station set-up and parameters, illustration (a) Map of Nigeria showing various soiling
 229 stations and their coordinates, (b) regions of soiling station as illustrated on the map, (c) soiled coupons
 230 samples, (d) transportation crate accommodating three samples with its cover, (e) typical soiling station
 231 set-up, (f) coupon dimension, and (g) sketch of deployed research jig.

232

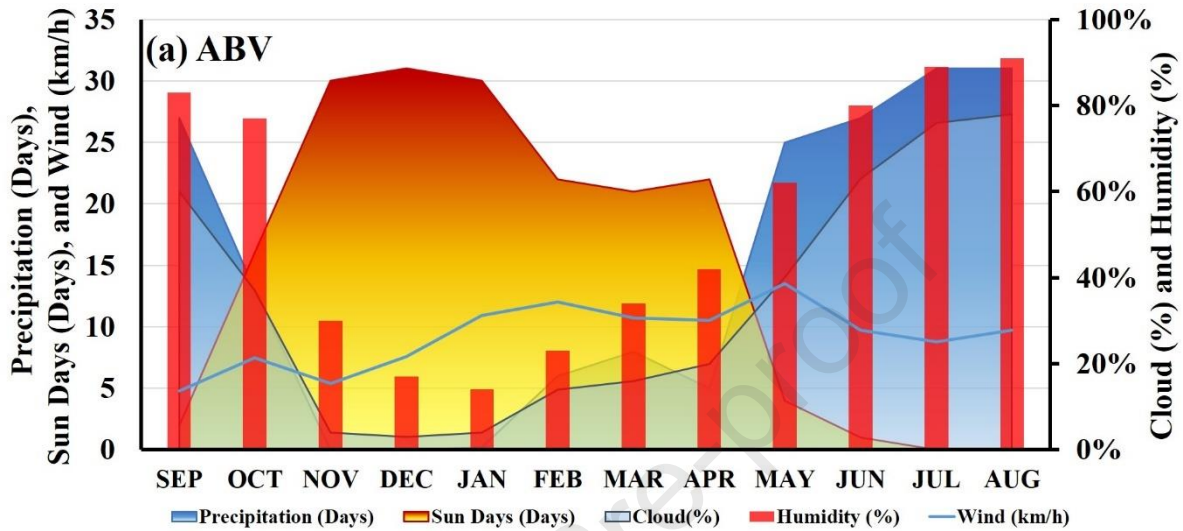
233 Javed et al. [31] reported that wind speed and humidity are the two most interactive variables that
 234 determine the rate at which airborne dust particles settle on a platform. The soiling stations' sites
 235 provide monthly average weather data (precipitation, sunny days, cloud, humidity, wind, and visibility)

236 of the soiling stations sites are also provided in Fig. 2, used for analysis purposes in this report. The
 237 weather data showed periods when the dry, dusty weather condition occurred and periods when
 238 precipitation (mainly rainfall) happened, which can sometimes assist in removing or reducing the
 239 accumulated dust.

240

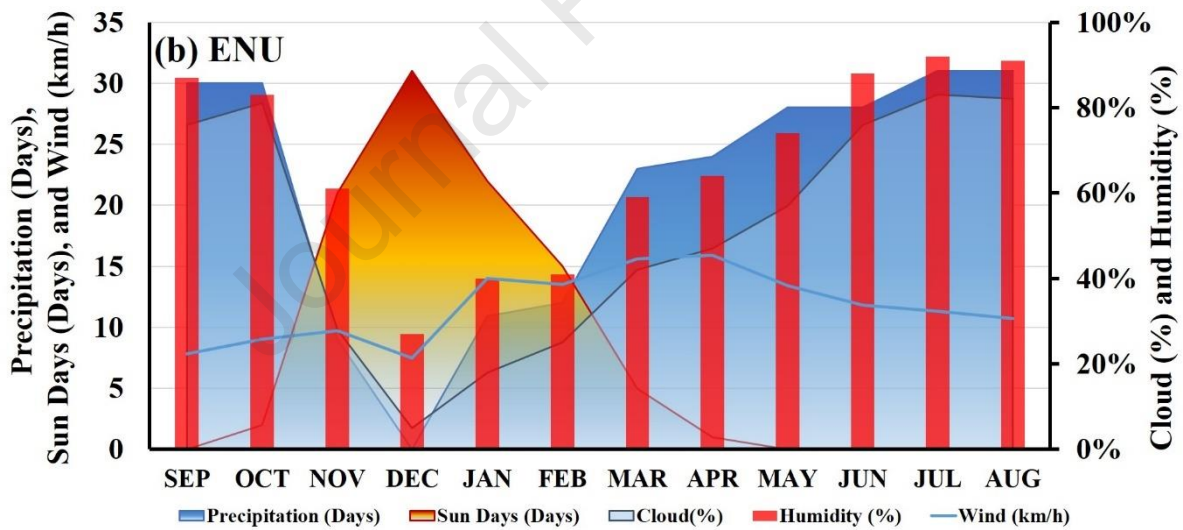
241 The influence of wind was minimised by installing all soiling stations in a pattern where coupons are
 242 forward-facing to each region's dominant incoming wind direction. This allows similarity of data
 243 collection across sites.

244



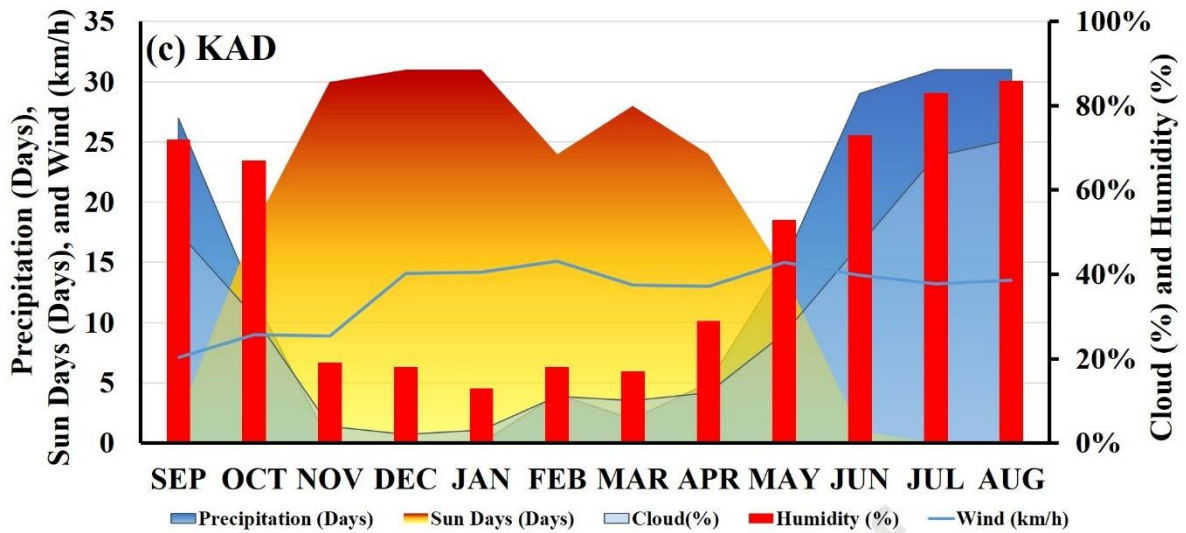
245

246

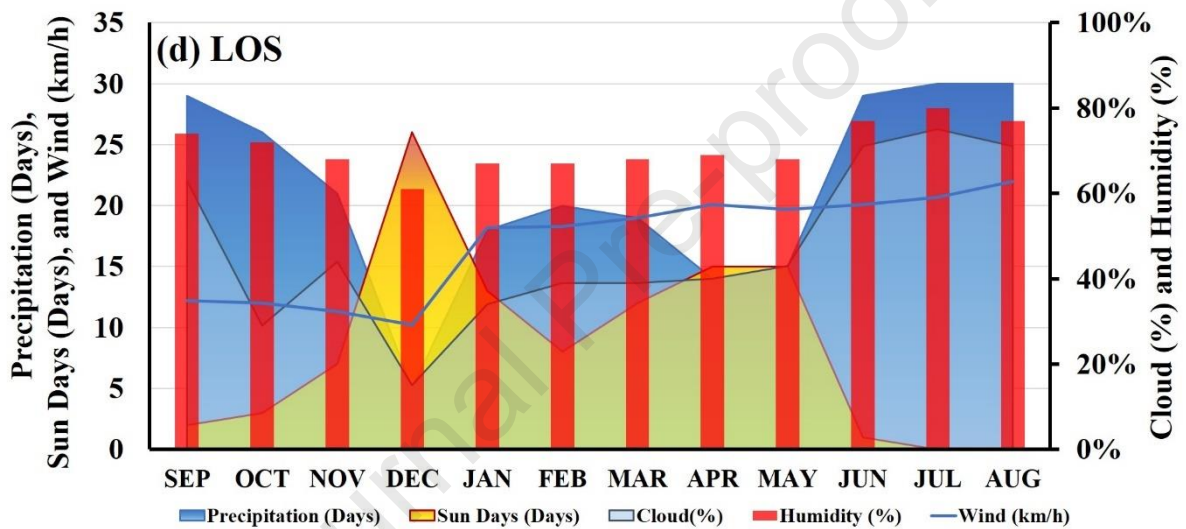


247

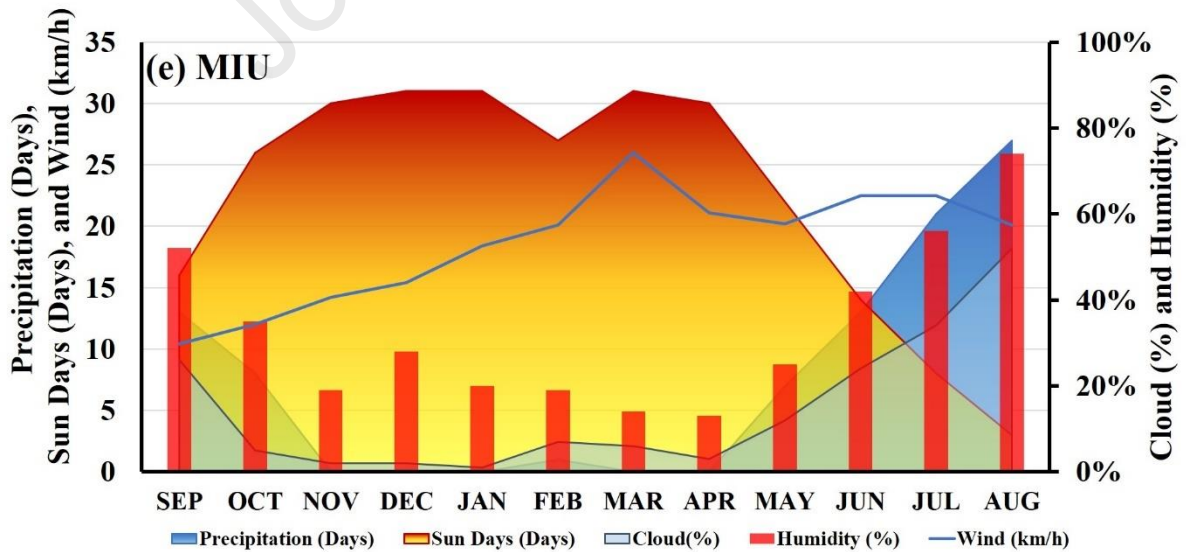
248



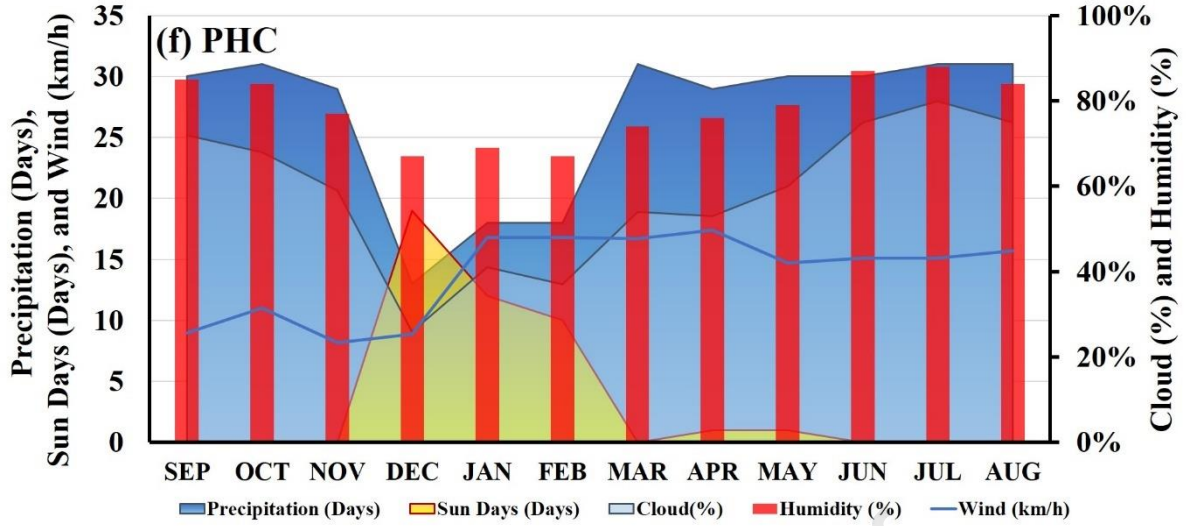
249
250



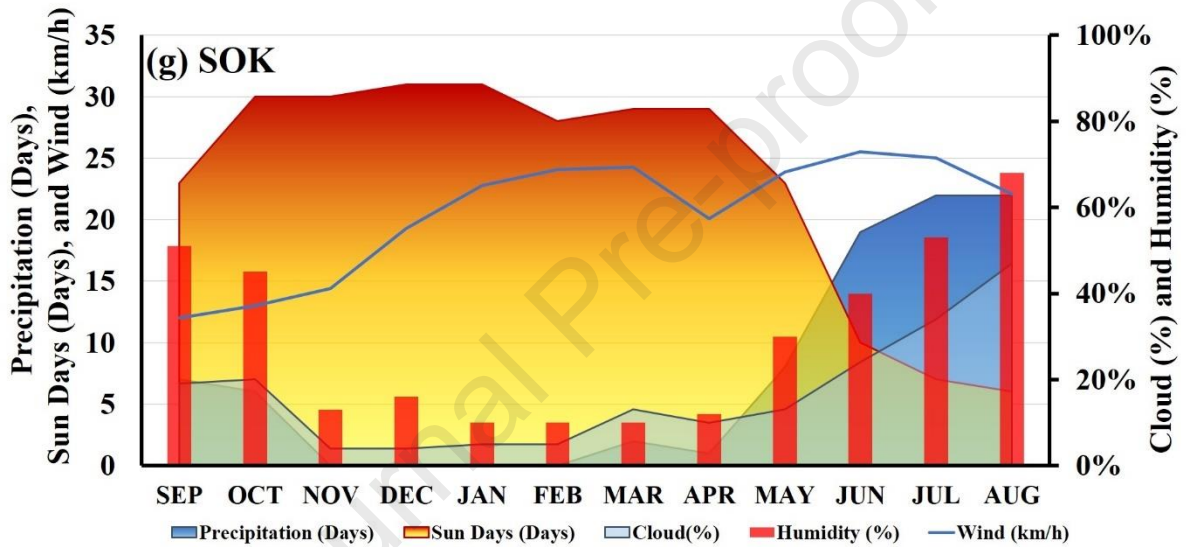
251
252



253
254



255
256



257

258

259

260

261

262

263

2.1 Optical characterisation procedure

264

265

266

267

268

269

270

271

272

273

274

275

276

Fig. 2: Monthly weather information variation for soiling stations illustrating precipitation, wind speed, sun days/month, relative humidity, and cloud (weather data obtained from World Weather Online[32]) for (a) – Abuja, (b) – Enugu, (c) – Kaduna, (d) – Lagos, (e) – Maiduguri, (f) – Portharcourt, and (g) - Sokoto.

The spectral characterisation was conducted to define the transparency level of the accumulated dust particles on the various coupons. This experiment was conducted when samples were brought back to the University of Exeter laboratory. Perkin Elmer Lambda 1050 UV/VIS/NIR spectrophotometer examined each exposed coupon. A clean coupon was usually examined at the beginning of every test to benchmark the optimum transmittance level that could be achieved. Afterwards, each sample was then subjected to a transmittance measurement. NIR (Near Infra-Red), VIS (Visual) and UV (Ultraviolet) transmittance levels of each coupon are examined, ranging from 300 nm to 1100 nm wavelength. This range of wavelength is considered to be accommodating all the different PV technologies (solar cells) available in the market as they respond only within this spectrum. Results obtained in this experiment were validated using Equation (1) below, where $S(\lambda)$ is the relative solar radiation wavelength distribution, $\Delta\lambda$ is the change in wavelength, and $T(\lambda)$ is the spectral transmittance.

$$\tau_{solar} = \frac{\sum_{\lambda=300nm}^{1100nm} S(\lambda)T(\lambda)\Delta\lambda}{\sum_{\lambda=300nm}^{1100nm} S(\lambda)\Delta\lambda} \quad (1)$$

277

278 Transmittance losses were calculated using Equation (2) below, and the extreme optical loss results
 279 were used instead of average to accommodate a possible worst-case scenario. The results are presented
 280 in percentage reduction, where τ_{clean} is the transmittance data of clean coupons and τ_x is the
 281 transmittance data of an exposed coupon on a certain angle.
 282

$$\Delta\tau_x = \frac{(\tau_{clean} - \tau_x)}{\tau_{clean}} (\%). \quad (2)$$

283
 284 This Equation (2) provided data employed in obtaining the power reduction of a kWp installation due
 285 to soiling. A simple approach to determining soiling losses, where reduction is determined by
 286 multiplying PV yield of kWp by the factor of (1-loss), where the loss refers to the percentage change in
 287 optical transmission obtained by employing Equation (2). This approach with simplicity would allow
 288 repeatability in other regions to determine soiling loss value.
 289

290 **2.2 Particle characterisation**

291 The sample particle characterisation was conducted to determine the chemical composition of dust
 292 particles in various soiling stations. One coupon with a high accumulation from the various soiling
 293 stations was carefully selected and exposed to imaging characterisation. Each sample was initially
 294 prepared with carbon coating using an Emi-Tech K950 device before being subjected to microscopic
 295 scanning. The SEM (S) Quanta FEG 650 was employed to generate the secondary electron (SE) image
 296 and backscattered electrons (BSE) image that was used for further mineral data acquisition using the
 297 EDX (Energy Dispersive X-ray). The EDX generated graphs highlighting mineral element's samples
 298 and their content level, which helped identify the various minerals' chemical composition. Minerals and
 299 their morphological characteristics such as diaphaneity were identified using online minerals databases
 300 such as minerals.net, mindat.org and webminerals.com.
 301

302 Additional information regarding the air quality of various regions in Nigeria was obtained from the
 303 Air Plume lab. The data were required for in-depth analysis of suspended particles in the atmosphere
 304 across the various regions. Air quality data highlights the aerosol particles' categories used to analyse
 305 and validate the minerals recorded from the SEM/EDX imaging and analysis. Annual average AQI
 306 highlights the severity of the harmfulness of atmospheric particles to humans using an innovative
 307 standard developed by Air Plume Lab [33] with seven different levels to eliminate the variability of
 308 different standards and also align with the World Health Organisation (WHO) recommended threshold
 309 is presented in a map format in Supplementary Fig. 17. The number of days considering the severity of
 310 harmfulness of air quality in the various regions is illustrated in Supplementary Fig. 18.
 311

312 **2.3 Soiling mapping procedure**

313 This is an approach for presenting PV soiling data. The coupon's transmittance data was collected from
 314 optical characterisation through spectral measurement using a spectrometer, as mentioned in section 2.1
 315 of this paper. PV output and direct normal irradiance data were collected from Global Solar Atlas,
 316 considering the small residential capacity of 1kWp. These data were used in calculating soiling losses,
 317 and the results were presented innovatively for easy understanding and further application. Linear
 318 interpolation was employed to determine the optical transmittance degradation of each soiling site's
 319 optimum PV tilt angle since coupons were not positioned at that angle. This interpolation technique
 320 was considered since it could establish a data point whenever established discrete data points, where
 321 $\Delta\tau_{(Optimum)}$ is the calculated change of transmittance of a coupon at an optimum angle, $\beta_{(x)}$ is the
 322 optimum tilt angle of a particular station, $\beta_{(45)}$ is the tilt angle described as tilt angle in this research
 323 where coupons are positioned as tilt which is 45° , $\beta_{(0)}$ is the horizontal angle at which a coupon is
 324 positioned on the research jig in soiling stations, $\Delta\tau_{(0)}$ is the optical loss recorded on a coupon
 325 positioned on a horizontal plane, and $\Delta\tau_{(45)}$ is the optical loss recorded on the coupon positioned on the
 326 tilt angle plane (45°).
 327

$$\Delta_{\tau_{(Optimum)}} = \frac{(\beta_{(x)} - \beta_{(45)}) (\Delta_{\tau_{(0)}} - \Delta_{\tau_{(45)}})}{(\beta_{(0)} - \beta_{(45)})} + \Delta_{\tau_{(45)}} \quad (3)$$

328

329 ArcMap 10.6.1 from ArcGIS was employed to design the soiling map using the PV output and soiling
 330 losses data. An interpolation method called Kriging interpolation was employed, based on Equation (4)
 331 below Venkatramanan et al. [34] provided. The Kriging interpolation is a geostatistical method that
 332 provides smooth estimates to determine an unknown spatial value of a location. Venkatramanan et al.
 333 [34] defined Kriging interpolation as the best technique for unbiased linear estimation of unknown
 334 spatial values and temporal variables, where Z_K^* is the smooth estimate produced by Kriging
 335 interpolation, λ_i is the weight for Z_i , which is to ensure unbiasedness of the estimation, and Z_i is the
 336 variable.

337

$$Z_K^* = \sum_{i=1}^n \lambda_i Z_i \quad (4)$$

338

339 Equation (5), provided by Venkatramanan et al. [34], represents the unbiased condition of kriging
 340 interpolation, where Z_V is the actual value and the Z_K^* is the calculated estimated value, which is:

341

$$E \{Z_V - Z_K^*\} = 0 \quad (5)$$

342

343 Equation (6), provided by Venkatramanan et al. [34], shows the summation of the weight (λ_i) which
 344 is:

345

$$\sum_{i=1}^n \lambda_i = 1.0 \quad (6)$$

346

347 Equation (7), provided by Venkatramanan et al. [34], shows the estimation variance of Kriging
 348 interpolation, where $\bar{C}(V, V)$ is the covariance between the variables of the samples, μ is the Lagrange
 349 parameter, $\bar{C}(v_i, V)$ is the covariance between the estimations and the variables of the samples, which
 350 is:

351

$$\sigma_K^2 = E \{[Z_V - Z_K^*]^2\} = \bar{C}(V, V) + \mu - \sum_{i=1}^n \lambda_i \bar{C}(v_i, V) \quad (7)$$

352

353 Equation (7) is provided to explain how the errors are reduced when estimating the values of Equation
 354 (5), which is a further description of the Kriging interpolation equation provided above in Equation (4).

354

355 The calculated soiling losses variation presented in Fig. 6 provided the disparity between the result
 356 obtained from this study and the GSA PV yield using a constant value of 4.5% data. The difference
 357 between the two values is that higher disparities were observed with increased soiling losses value. It
 358 also increases with time since more irradiance is available to generate PV yield, and the 4.5% soiling
 359 losses constant would not change with time. Therefore, it will create a broader gap of soiling losses as
 360 the duration increases, and soiling losses increase due to a significant amount of irradiance that was not
 361 converted to useful energy.

362

363 ArcMap from ArcGIS is a software that provides the platform to present geographic information in
 364 layers and could be used to perform a wide range of GIS-related tasks, including compilation,
 365 organisation, and modification of GIS datasets, use of geoprocessing for analytical and visual purposes
 366 [18]. The application is mainly used by government administrative established compared with MapBox,
 367 leaflet, and Google and has the highest market share in the mapping application industry [19]. This
 368 application was employed in this study because it provides flexibility to create and edit datasets. The
 369 application is secured and requires a license for online access that allows users to load required real-
 370 world geographical information data [20]. Three software (ArcGIS, MapBox, and Tableau) were

371 employed to develop the mapping, but the result was better achieved using ArcGIS because of the
 372 advanced inbuilt tools that support the modification of datasets.

373

374 The Kriging interpolation technique is an advanced geostatistical approach that generates an estimated
 375 surface from a given scattered set of points with z-values [21]. This technique uses an interactive
 376 investigation of the spatial behaviour of the inputted data to select an excellent estimation for output
 377 generation. Desktop.ArcGIS [21] provided a multistep process for Kriging interpolation, including
 378 exploratory statistical data analysis, variogram spatial structural modelling, creating the surface, and
 379 exploring surface variation. The main dissimilarity with other spatial interpolation techniques in
 380 ArcGIS, such as the inverse distance weighted (IDW) and Spline interpolation, is that it is not a
 381 deterministic approach based on surrounding values but a geostatistical approach that is based on a
 382 statistical model which includes autocorrelation, where it could produce a significant measure of
 383 accuracy during predictions [21]. Krishnan and Ganguli [22] reported that the Kriging interpolation
 384 model could provide higher accuracy and lower computational cost for predicting distribution spatial
 385 frequencies compared to other deterministic techniques. Zhang et al. [23] reported that kriging model
 386 fitting accuracy could reach up to 0.980. Fischer et al. [24] supported this claim by examining three
 387 interpolation techniques (inverse distance weighted, ordinary Kriging, and Empirical Bayesian
 388 Kriging), and the ordinary Kriging consistently yielded more accurate results than others. The technique
 389 assumes the distance of sample points reflects spatial correlation to explain surface variance. It uses all
 390 points provided to generate output in a specified radius using a mathematical function of unbiasedness
 391 [18]. Based on this literature and a comparative assessment using the GSA map and its data (direct
 392 normal irradiance and PV performance with 4.5% soiling rate), the accuracy of IDW and Kriging were
 393 investigated, and our finding shows that Kriging interpolation provides better map output than is more
 394 similar to the GSA map. As such, the technique was employed for generating soiling maps.

395

396 This novel approach is motivated by recent progress made by GSA in providing solar energy
 397 information, which could be improved by adopting the method used in this study since it offered a low-
 398 cost soiling station that could be used to determine the actual regional soiling loss. The approach could
 399 stimulate further soiling research across the globe and reduce the inaccuracy reported. The paper
 400 contributes to the body of knowledge with the unique, low-cost approach used to determine the soiling
 401 rate, which policymakers can use, PV companies, researchers, and potential PV investors. The findings
 402 from this study may lead to a better understanding of soiling problems since the work highlights the
 403 significance of the effect of soiling, considering environmental differences as an influencing factor. The
 404 findings provided more accurate and realistic soiling information for better PV installation and
 405 maintenance planning to achieve higher yields.

406

407 **3 Results**

408 The spectrophotometer was employed to measure the transmittance losses on coupons, scanning
 409 electronic microscope/ energy dispersive X-ray (SEM/EDX) was used to determine the soiled particles'
 410 chemical composition ArcGis (ArcMap 10.6.1) was employed to develop a soiling losses map. All the
 411 results are illustrated in this section.

412

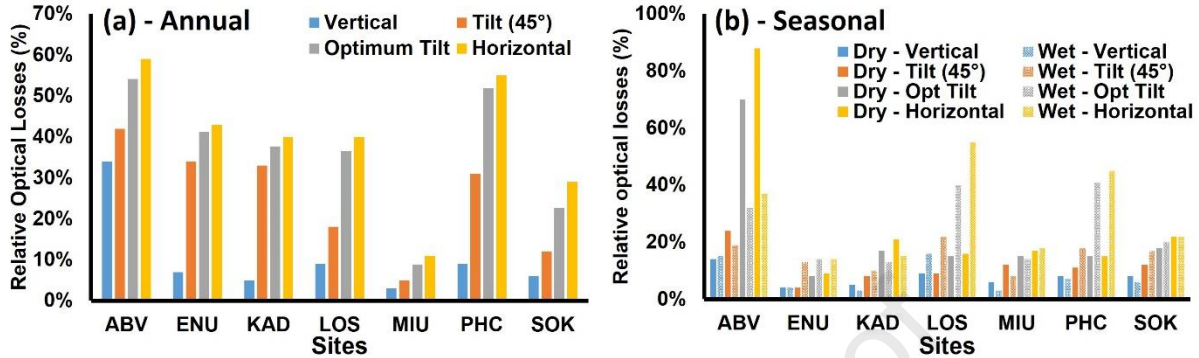
413 **3.1 Optical transmittance losses**

414 The optical losses results are grouped by exposure period, and each group is further divided into
 415 subgroups based on their positioning angles. This illustrates transmittance losses of various locations at
 416 a glance for better understanding. Graph plots illustrating relative optical losses variation relative to
 417 wavelengths of all exposed coupons are provided in the supplementary figures section from
 418 Supplementary Fig. 1 to Supplementary Fig 15. Below charts were provided to highlight relative
 419 changes.

420

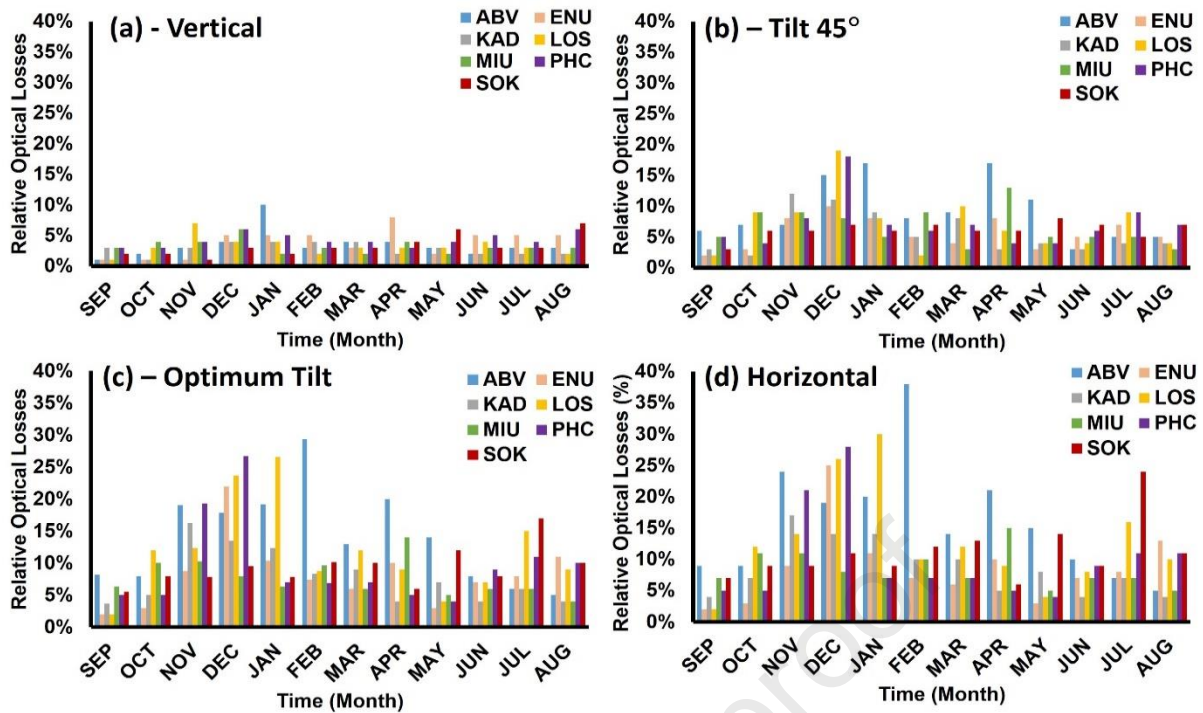
421 Fig. 3 (a) illustrates the annual transmittance loss results. The most significant loss of about 59% was
 422 recorded on the Abuja (ABV - 08°59'25", 07°21'34") coupon that was positioned on a horizontal plane,
 423 while the lowest loss was about 3% and was recorded on the Maiduguri (MIU - 11°51'08", 13°05'03")
 424 coupon that was positioned at a vertical angle. Fig. 3 (b) illustrates the dry season transmittance loss
 425 results where the 88% loss was recorded for the horizontally placed ABV coupon, while the lowest loss
 426 is about 4% from the vertically placed Enugu (ENU - 06°51'57", 07°24'58") coupon. On the other hand,

427 Fig. 3 (b) illustrated wet season transmittance losses, and the most significant losses were recorded from
 428 Lagos (LOS - 06°35'00", 03°20'00") and Port Harcourt (PHC - 05°00'29", 06°57'02") coupons
 429 positioned on horizontal planes, with the first having about 55% reduction and the latter having about
 430 45%. The lowest transmittance losses for the wet season were recorded from Kaduna (KAD - 10°30'59",
 431 07°26'38") and MIU coupons, with both having about a 3% reduction when coupons were positioned
 432 vertically. Sokoto (SOK - 13°07'59", 05°12'13") coupons appear average in all positions.
 433



434 Fig. 3. (a) Annual optical transmittance losses variation for vertical, 45° tilt, and horizontal orientation.
 435 At the same time, (b) illustrates seasonal optical transmittance losses variation for vertical, 45° tilt, and
 436 horizontal orientation, with Dry highlighting dry seasonal variations and Wet showing wet seasonal
 437 variations for the seven regions.
 438
 439

440 Fig. 4 (a) illustrates monthly results from coupons that are vertically positioned, with the lowest optical
 441 losses of about 1% in September (for ABV, ENU, and LOS), October (for ENU and KAD), and
 442 November (SOK). Fig. 4 (a) further illustrates the optical loss recorded for the vertically positioned
 443 coupons, with a maximum of 10% in January (for ABV). Fig. 4 (b) illustrates results from coupons that
 444 are positioned at 45° tilt, with the lowest optical losses of about 2% in September (ENU and LOS),
 445 October (for KAD), and February (LOS). Fig. 4 (b) further illustrates the maximum loss for the 45° tilt
 446 position, with about 19% in December (for LOS). Fig. 4 (c) illustrates optical loss results of each site's
 447 optimum tilt calculated from the interpolation between horizontal and 45° tilt relative transmittance
 448 reductions, with the lowest optical loss of about 2% in September (for ENU and LOS). Fig. 4 (c) further
 449 illustrates the maximum loss for the optimum tilt angle position, with about 29% in February (for ABV).
 450 Fig. 4 (d) illustrates results from horizontally positioned coupons, with the lowest optical losses of about
 451 2% in September (ENU and LOS). Fig. 4 (d) further illustrates the maximum loss for the horizontal
 452 position, with about 38% in January (for ABV).
 453



454
 455 Fig. 4. Variation of monthly optical transmittance losses in relation to the angular position of coupon
 456 with respect to the terrain as the reference point (=0); where (a) Vertical (90°), (b) Tilt (45°), (c)
 457 optimum tilt angle for the exposure site, and (d) horizontal (0°). (a) illustrates higher accumulation was
 458 recorded in January (on the ABV coupon), and most minor were recorded in September (on ABV, ENU,
 459 and LOS coupon), October (ENU and KAD coupon) and November (SOK and ENU coupon) for the
 460 vertically positioned coupons. (b) shows the most increase was recorded in December (on the LOS
 461 coupon), and the most minor were recorded in September (on ENU and LOS coupon), October (on
 462 KAD coupon) and February (LOS) for 45° positioned coupons. (c) depicts the calculated optical losses
 463 value with the most significant accumulation recorded in February (on the ABV coupon), and the most
 464 minor were recorded in September (on KAD and LOS coupons) for coupons positioned at a site-specific
 465 optimal angle. (d) demonstrates that the most significant accumulation was recorded in February (on
 466 the ABV coupon), and the most minor were recorded in September (on ABV) for horizontally
 467 positioned coupons.

468 3.2 Particle characterisation

469 This section presents the results of the SEM/EDX scanings. SEM images of particle samples with their
 470 various locations, highlighting the sizes and spaces they occupied on the coupons, are provided in
 471 Supplementary Fig. 16. However, the backscattered electron images (BSE) were employed for in-depth
 472 analysis to determine the mineral composition using EDX. Data obtained from the EDX analysis were
 473 employed to identify the essential mineral and their characteristics using the online mineral data
 474 databases such as minerals.net, mindat.org and webminerals.com.
 475

476 A critical property (diaphaneity) of each identified mineral was investigated, and some of the minerals
 477 possess a characteristic that would negatively affect light transmittance. Table 2 highlights some
 478 minerals that were repeatedly identified during the particle characterisation. The results from the
 479 Northern region show the diaphaneity property of some of the minerals where the coupons from North-
 480 East appear to be translucent and opaque, and coupons from North-Central possess minerals found to
 481 have translucent and opaque properties. In contrast, the coupons from North-West appears to have
 482 minerals with both transparent and translucent property. In the Southern region, Table 2 shows that the
 483 coupon from the South-East possesses minerals that appear to be transparent, translucent, and some are
 484 opaque. The particles on the South-South coupon have minerals with opaque properties, while the
 485 minerals identified on the South-West coupon possess translucent and opaque transparency properties.
 486 Table 2. illustrates the Air Quality Index (AQI) of various regions and the main pollutants.
 487

488

489 Table 2. Soiling stations with coordinates, fixed optimum angular PV positioning with the recorded
 490 Mineral and their transparency characteristics, and the AQI/PM data obtained from Air Plum Lab.
 491

S/N	Location Region Latitude Longitude Optimum PV Tilt Angle (OPTA)	Minerals	Diaphaneity	Annual Average Best day Worst day	Main Pollutant	
					AQI	$\mu\text{g}/\text{m}^3$
1.	ABV (Abuja) North Central 08°59'25" 07°21'34" OPTA - 13°	Chlorite (Chamosite)	Translucent to sub-translucent	75 AQI Best - 17 AQI Worst - 330 AQI	PM ₁₀ - 343.7	PM ₁₀ - 469.9
		Montmorillonite	Translucent to Opaque		PM _{2.5} - 399.8	PM _{2.5} - 349.8
		Pyroxene (Spodumene)	Transparent to Translucent		SO ₂ - 6.6	SO ₂ - 6.6
					CO - 9.98	CO - 1997.8
					O ₃ - 111.6	O ₃ - 178.5
					NO ₂ - 19.3	NO ₂ - 38.6
2.	ENU (Enugu) South East 06°51'57" 07°24'58" OPTA - 10°	Tourmaline (Dravite)	Translucent to opaque	75 AQI Best - 16 AQI Worst - 399 AQI	PM ₁₀ - 450.7	PM ₁₀ - 641.1
		Analcite	Translucent		PM _{2.5} - 524.9	PM _{2.5} - 474.9
		Pectolite	Transparent to Translucent		SO ₂ - 21.1	SO ₂ - 24.0
					CO - 22.2	CO - 4398.1
					O ₃ - 111.6	O ₃ - 178.5
					NO ₂ - 46.7	NO ₂ - 75.5
3.	KAD (Kaduna) North West Main Base 10°30'59" 07°26'38" OPTA - 15°	Tourmaline	Translucent to opaque	96 AQI Best - 22 AQI Worst - 388 AQI	PM ₁₀ - 415.8	PM ₁₀ - 585.3
		Chlorite (chamosite)	Translucent to sub-translucent		PM _{2.5} - 394.7	PM _{2.5} - 344.7
		Garnet (almandine)	Transparent to Translucent		SO ₂ - 32.1	SO ₂ - 62.5
					CO - 15.9	CO - 3181.8
					O ₃ - 94.6	O ₃ - 153.5
					NO ₂ - 26.9	NO ₂ - 49.2
4.	LOS (Lagos) South West 06°35'00" 03°20'00" OPTA - 7°	Stilpnomelane	Subtranslucent to opaque	65 AQI Best - 14 AQI Worst - 392 AQI	PM ₁₀ - 322.3	PM ₁₀ - 435.7
		Beryl	Transparent to subtranslucent		PM _{2.5} - 336.4	PM _{2.5} - 286.4
		Amphibole	Translucent to Subopaque		SO ₂ - 51.97	SO ₂ - 133.9
					CO - 72.1	CO - 8278.8
					O ₃ - 170.96	O ₃ - 273.5
					NO ₂ - 73.7	NO ₂ - 136.9
5.	MIU (Maiduguri) North East 11°51'08" 13°05'03" OPTA - 17°	Zeolite (Clinoptilolite)	Transparent	117 AQI Best - 21 AQI Worst - 562 AQI	PM ₁₀ - 362.9	PM ₁₀ - 500.5801
		Ilmenite	Opaque		PM _{2.5} - 455.6	PM _{2.5} - 405.5584
		Illite	Translucent		SO ₂ - 12.6	SO ₂ - 12.57944
					CO - 8.9	CO - 1783.942
					O ₃ - 90.8	O ₃ - 148.9783
					NO ₂ - 19.4	NO ₂ - 38.81303
6.	PHC (Port Harcourt) South-South 05°00'29" 06°57'02" OPTA - 6°	Felspar (albite)	Transparent, Translucent	62 AQI Best - 13 AQI Worst - 321 AQI	PM ₁₀ - 322.2	PM ₁₀ - 435.555
		Schorlomite	Opaque		PM _{2.5} - 367.1	PM _{2.5} - 316.4977
		Scapolite	Translucent to Opaque		SO ₂ - 32.5	SO ₂ - 63.86763
					CO - 17.7	CO - 3546.805
					O ₃ - 122.8	O ₃ - 196.5006
					NO ₂ - 41.4	NO ₂ - 68.52894
7.	SOK (Sokoto) North West 13°07'59" 05°12'13" OPTA - 17°	Chlorite (Chamosite)	Translucent to subtranslucent	95 AQI Best - 20 AQI Worst - 418 AQI	PM ₁₀ - 557.2	PM ₁₀ - 811.6
		Montmorillonite	Translucent to Opaque		PM _{2.5} - 369.7	PM _{2.5} - 319.7
		Feldspar (labradorite)	Translucent to transparent		SO ₂ - 14.1	SO ₂ - 14.1
					CO - 12.3	CO - 2453.1
					O ₃ - 128.1	O ₃ - 205.1
					NO ₂ - 42.1	NO ₂ - 68.3

492
493

3.3 Soiling mapping

494 In combination with PV Output data obtained from the Global Solar Atlas, the transmittance losses
 495 were used to develop a new soiling losses map for Nigeria. Since the PV output collected from Global
 496 solar was based on the optimum angle of each location, a linear interpolation was employed to obtain
 497 optimum angle optical transmittance losses data, which is comprehensively explained in the
 498 methodology section of this paper. PV output data with and soiling losses are provided according to the
 499 timestamp for annual in Table 3, for the two seasons (dry and wet) in Table 4, and for various 12
 500 calendar months in Table 5

501
 502 The soiling maps are grouped based on the period of exposure, and each group includes a direct normal
 503 irradiance [16], PV output without soiling, and PV output at a fixed position based on the site's optimum
 504 PV tilt angle (provided in Table 1) with soiling based on the transmittance losses data presented above,
 505 and the PV output with a constant 4.5% soiling loss map [16]. This is employed to illustrate solar energy
 506 potential and the variation between the result of this study and the information provided on the Global
 507 Solar Atlas website.

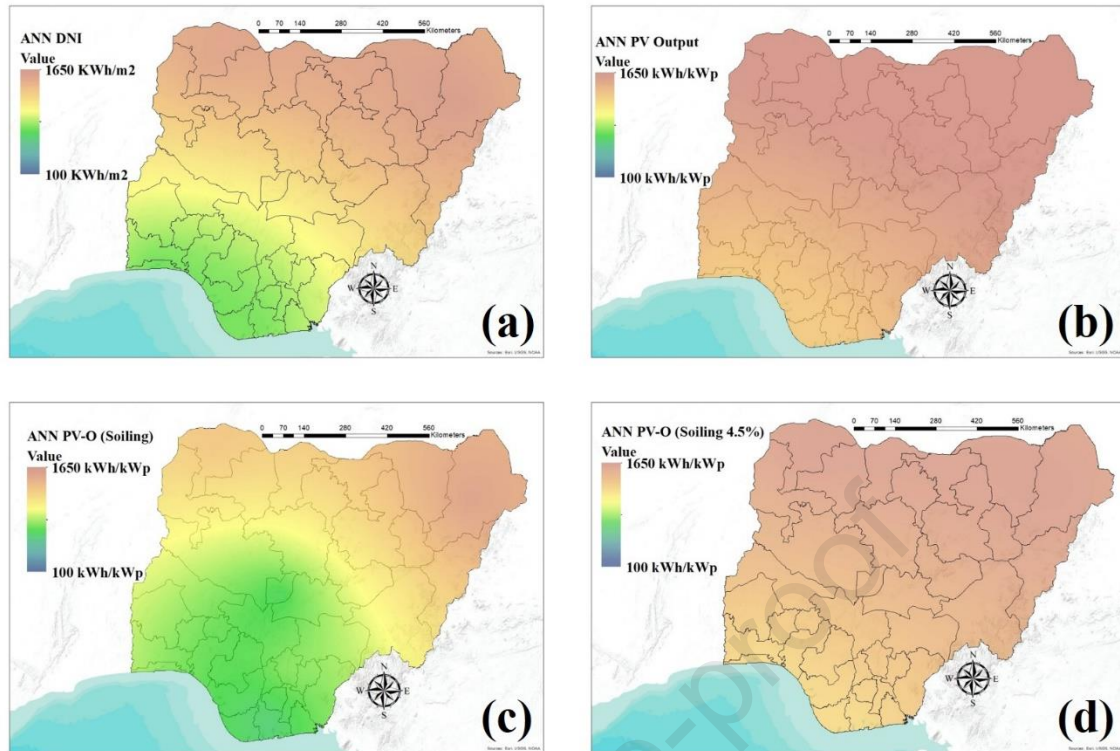
508

509 Table 3. Estimated annual PV output with and without soiling losses for seven sites.

Annual PV output (kWh/kWp)		
STATE	Without Soiling	With Soiling
ABV	1506	691
ENU	1399	823
KAD	1623	1012
LOS	1299	824
MIU	1706	1555
PHC	1304	628
SOK	1695	1313

510

511 Fig. 5 (c) shows that the most significant soiling loss was recorded in North-Central, where the PV
 512 output degraded from about 1505.76 kWh/kWp to 691.3 kWh/kWp (54% loss), and the lowest loss was
 513 recorded in the North-East region where PV output decreased from 1705.76 kWh/kWp to about 1554.52
 514 kWh/kWp (9% loss). In comparison, the maps presented in Fig 5 distinguish the variation between a
 515 constant soiling value (of 4.5 %) and actual soiling losses values for a wider region. The reader could
 516 easily observe a wider variation when comparing the values from the maps in Fig. 5 (b) and Fig. 5 (d),
 517 where an additional 50% loss was recorded for the North-Central region. Fig. 5 (d) illustrates that the
 518 greatest loss was recorded in the North-East region, where PV yield degraded from 1705.76 kWh/kWp
 519 to about 1629 kWh/kWp (4.5% loss), and the lowest reduction was in the South-West where the
 520 reduction was from 1299.48 kWh/kWp to about 1241 kWh/kWp (4.5% loss). Although the loss
 521 percentage is constant, it is observed that losses are greater in regions with higher potential. In
 522 comparison, the reader could easily observe a wider variation when comparing the values from the maps
 523 in Fig. 5 (b) and Fig. 5 (d), where an additional 25% loss was recorded for the North-Central region.



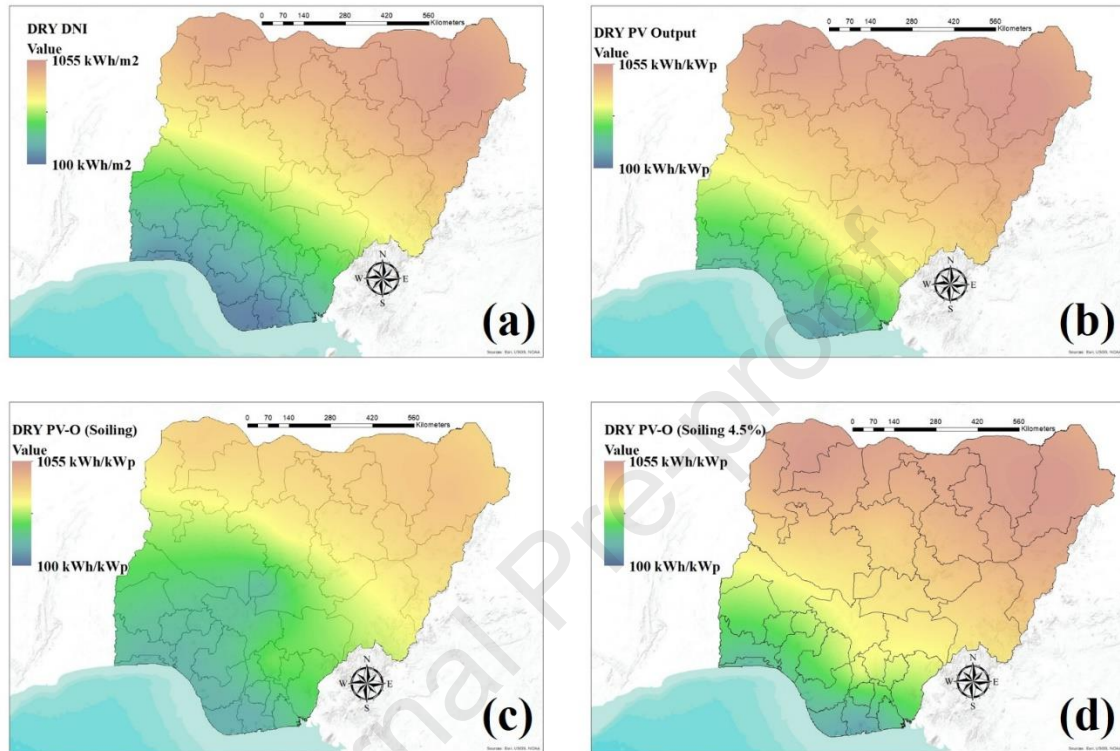
524 Fig. 5. Mapping annual regional variation of DNI (Direct Normal Irradiance) potential and PV output
 525 of Nigerian highlighting soiling losses disparity and showing significant soiling losses in the South-
 526 East, South-West, South-South, and North-Central with; (a) highlighting the annual solar energy
 527 potential of all the region in the country, (b) demonstrating the annual PV output potential with no
 528 soiling, (c) illustrating the annual soiling losses determined through optical losses, and (d) showing the
 529 annual PV output reduction due to constant soiling losses rate (4.5%).
 530
 531

532 Table 4. Estimated seasonal (dry and wet) PV output with and without soiling losses for seven sites.

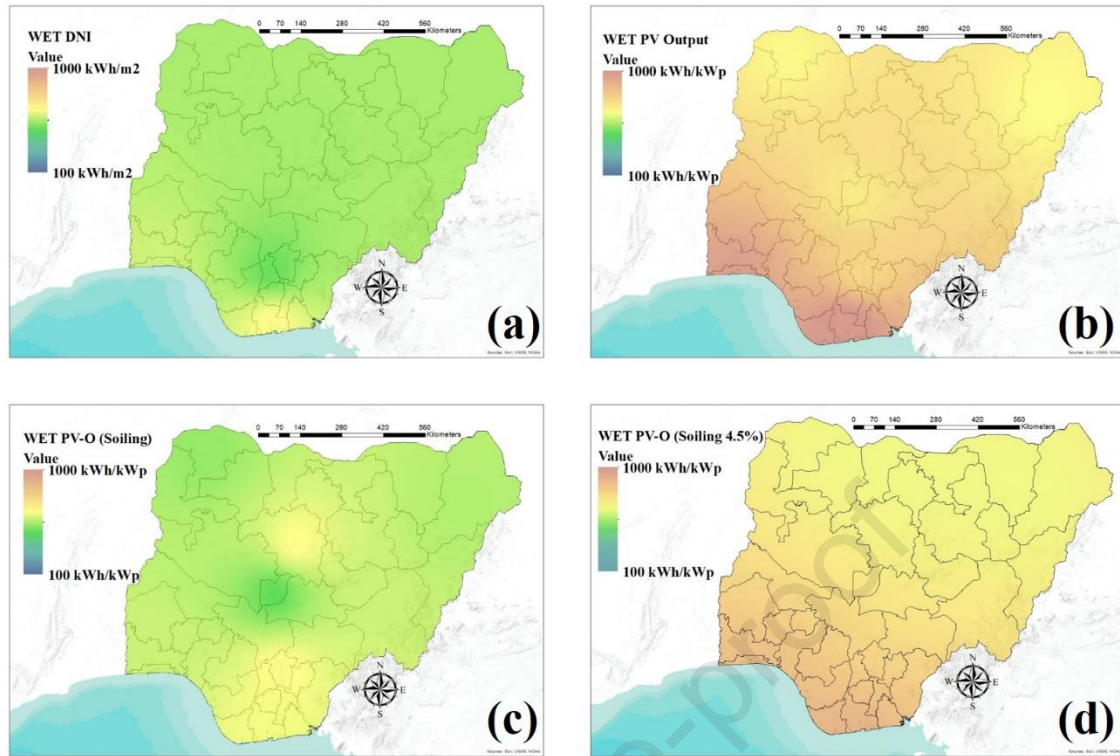
STATE	Seasonal PV output (kWh/kWp)			
	DRY		WET	
	No Soiling	Soiling	No Soiling	Soiling
ABV	819	246	687	467
ENU	646	594	753	648
KAD	884	733	740	644
LOS	336	286	964	578
MIU	1064	904	641	551
PHC	241	205	1063	627
SOK	1041	853	655	524

533
 534 The results of the seasonal soiling mapping show a significant variation in soiling losses during the two
 535 seasons across regions. Fig. 6 (c) illustrates the soiling losses in the dry season. It shows that in North-
 536 Central, the PV output decreased from about 818.53 kWh/kWp to 573.0 kWh/kWp (30% loss) and in
 537 the South-South from 240.6 kWh/kWp to about 204.5 kWh/kWp (14% loss). Fig. 6 (d) shows PV output
 538 reduction due to soiling losses where the most significant decrease was observed in the North-East
 539 region from 1064.1 kWh/kWp to about 1016.2 kWh/kWp (4.5% loss), and the lowest reduction was
 540 from South-South where the drop was from 240.6 kWh/kWp to about 229.8 kWh/kWp (4.5% loss). The
 541 approach used in the study presented a greater soiling value as shown in Fig. 6 (c), where about 245.53
 542 kWh/kWp reduction is obtained in North-Central compared to reduction illustrated in Fig. 6 (d) which
 543 shows 36.8 kWh/kWp using 4.5% constant soiling value.
 544

545 On the other hand, Fig. 7 (c) shows that the most significant soiling loss in the wet season was recorded
 546 in South-South, where the PV output decreased from about 1063.4 kWh/kWp to about 627.4 kWh/kWp
 547 (41% loss) and the lowest loss was recorded in the North-East region where PV output reduces from
 548 641.3 kWh/kWp to about 551.5 kWh/kWp (14 % loss). Fig. 7 (d) shows the most significant reduction
 549 was recorded in the South-South region from 1063.4 kWh/kWp to about 1015.5 kWh/kWp (4.5% loss),
 550 and the lowest drop was from the North-East where the decrease was from 641.3 kWh/kWp to about
 551 612.4 kWh/kWp (4.5% loss).
 552



553
 554 Fig. 6. Mapping dry season regional variation of DNI (Direct Normal Irradiance) and PV output
 555 potential of Nigeria, highlighting soiling losses disparity during the season; (a) illustrates solar energy
 556 potential for the dry season in the country, (b) shows PV output potential for the dry season without
 557 soiling, (c) illustrates the PV yield with soiling losses for the dry season, and (d) shows the dry season
 558 PV output with constant soiling losses rate (4.5%).
 559



560
561 Fig. 7. Mapping wet season regional variation of DNI and PV output potential of Nigeria, highlighting
562 soiling losses disparity with (a) highlighting solar energy potential for the wet season in the country, (b)
563 demonstrating PV output potential for the wet season without soiling, (c) illustrating the PV yield with
564 soiling losses for the wet season, and (d) showing the wet season PV output with constant soiling losses
565 rate (4.5%).

566
567 The monthly result shows different values of soiling losses for each month. Consequently, the results
568 are shown in monthly-based maps. All monthly maps are illustrated in Supplementary Fig. 19 to
569 Supplementary Fig. 30. Table 5 provides the PV yield with and without soiling losses for the sites based
570 on kWp installation.

571
572 Table 5. Estimated monthly PV output with and without soiling losses for seven sites.

	PV output without soiling losses (kWh/kWp)											
STATE	SEP	OCT	NOV	DEC	JAN	FEB	MAR	APR	MAY	JUN	JUL	AUG
ABV	115	136	150	147	140	125	133	123	123	110	105	100
ENU	105	118	135	141	132	117	121	116	116	104	100	95
KAD	126	146	157	158	154	137	144	134	134	117	112	107
LOS	100	110	112	119	112	105	117	117	117	97	96	97
MIU	139	155	155	160	161	143	150	135	135	121	125	124
PHC	103	114	116	124	116	105	109	114	114	98	94	99
SOK	141	151	151	156	155	140	146	137	137	127	130	126
	PV output with soiling losses(kWh/kWp)											
STATE	SEP+S	OCT+S	NOV+S	DEC+S	JAN+S	FEB+S	MAR+S	APR+S	MAY+S	JUN+S	JUL+S	AUG+S
ABV	106	125	121	121	113	88	116	99	105	101	98	95
ENU	103	115	123	110	118	109	114	104	112	97	92	84
KAD	121	139	131	137	135	126	131	129	122	113	105	103
LOS	98	97	98	91	82	95	103	107	112	90	82	88
MIU	130	139	139	147	150	130	141	116	126	114	117	119
PHC	98	109	93	91	108	97	101	108	109	89	84	89
SOK	134	139	139	142	143	126	132	129	119	117	108	114

4 Discussion

The optical loss results presented in the previous section are percentage reductions from a cleaned, low iron glass coupon. This section summarises and discusses the key findings based on critical observation and evaluation of results considering additional parameters such as weather, atmospheric particle, and AQI presented in the methods section.

The transmittance losses values obtained from the results shown in the previous section highlighted a significant variation between a cleaned coupon and coupons exposed to outdoor weather conditions. The most intriguing finding considering the optical transmittance results in high losses identified in coupons position on the horizontal plane across all the soiling stations. The greatest soiling among the annual coupon was recorded in ABV, the weather condition throughout the year as shown in Fig. 2 (a), where the dry season is longer than the wet season, and the AQI appears to be very high shown in Table 2 and Supplementary Fig. 17. However, it has been observed that the main pollutants are not extremely dangerous based on the information provided in Supplementary Fig. 18, but most of them have a very devastating effect on light transmittance based on the mineralogy analysis.

Climatic conditions such as humidity, wind speed/ direction, temperature and precipitation play a vital role in influencing soiling, but it could sometimes tranquillise the accumulation. Correlating findings of the optical losses in Fig 4 (a) - (d) with Fig. 2 (a) – (g) shows that weather parameters significantly influence accumulation. Considering monthly variation for North-Central (ABV), it was observed that the greatest optical losses were recorded from the January coupon, where soiling is assumed to be influenced by the increase in humidity and low precipitation, as shown in Fig. 2 (a). In the South-East region (ENU), the highest accumulation was recorded when the precipitation (rain) was lowest and wind and humidity were low, as presented in Fig. 2 (b). The greatest optical loss recorded in North-West (KAD and SOK) and North-East (MIU) occurred when precipitation was zero or low, the humidity was low, and wind speed was averagely high, as shown in Fig. 2 (c) and (g). Most significant accumulation transpired in South-West (LOS) and South-South (PHC) when precipitation was lowest, the wind was low, and humidity was high, as shown in Fig. 2 (d) and (f). Conversely, the lowest accumulation that translated to low optical losses was recorded when precipitation turned to be the highest across all the regions, as shown in Fig. 2 (a) – (g).

The seasonal optical transmittance losses results are additional information necessary to understand better the consequences of soiling on PV. The result shows wide variation between the dry and wet seasons, with the dry season showing the most significant losses in the Northern region due to Saharan dust (during Harmattan season) and while the wet season presents more losses in the Southern part. A most significant optical loss was recorded during the dry season in ABV, which is related to massive ongoing construction activities in the federal capital territory (including road, rail, and building construction) [35]. On the other hand, the most significant optical loss recorded during the wet season was in PHC, which is related to the region's massive oil exploration activities. The high optical losses rate in the South part of the country during the wet season is due to the longer duration of the wet season, which comes with light rain that lasts for about nine months, as shown in Fig. 2 (f), because of its proximity to the Atlantic Ocean. Fig. 2 (a) shows that the wind speed in ABV is the lowest. The humidity is highest considering the Northern region and similarly for PHC in the Southern region, highlighting why more accumulation was recorded in ABV during the dry season and PHC during the wet season. More detailed information on the seasonal variation in the region causing soiling is presented in Chanchangi et al. [2].

Considering the monthly timestamp as an exposure period, the Optical losses result provides vital information that breaks down the soiling formation data into a period that can be employed in many applications such as research, installation planning, and maintenance planning. The results illustrated different optical losses each month, and the greatest was recorded on the ABV coupon installed on a horizontal plane in February. Other months such as November, December, January, and April also presented significant losses. According to weather data provided in Fig. 2 (a), (b), (c), (d), (e), (f), and (g); all the above months tend to fall within the dry season with an influx of the Saharan desert that sweep the country. The atmospheric particles are blown away by the low-level jet (North-easterly)

628 winds from the far North (Northeast and Northwest) to the Northcentral and then the Southern part of
629 the country, causing high formation on surfaces in the Northcentral since the wind speed tends to drop
630 around the region. AQI tends to be very high during these dry months across the country, but the
631 cumulative annual average would end up very low. The AQI and the main pollutant AQI might be very
632 high in some regions, and the soiling level would be shallow; the high wind does not allow settlement
633 on platforms.

634

635 The angular variation of optical losses might be assumed to be always in the same pattern, where the
636 most significant losses should always be recorded on the horizontal plane, and the losses reduce as the
637 angle changes towards the vertical plane. However, it has been reported by Gholami et al.[36] that
638 dominating incoming wind could significantly influence the adhesion and accumulation of particles in
639 various angles, resulting in a disparity to the above assumption and a variation in the optical losses
640 result obtained from this study. The greatest optical loss is not continually expected to be obtained at
641 the horizontal plane all the time and in the entire region since the dominant wind direction could play a
642 significant role in the resuspension of deposited particles from a coupon. In addition, the optical losses
643 in correlation with angular variation presented in this study provide data that could be used for loss
644 correction of various angles when installations are to be made on angles other than the ones provided.
645 It is also to accommodate other PV applications, as earlier presented.

646

647 SEM/EDX analysis assisted in validating the optical losses by highlighting minerals that can absorb,
648 attenuate, or scatter light to penetrate them. Table 2 presents SEM/EDX results showing that some of
649 the particles on ABV's coupon are translucent and opaque, which could reduce light penetration. A
650 significant amount of dust accumulated on the coupon because the wet weather condition (light rain in
651 February) created cementation and lower wind velocity. A mineral particle such as Montmorillonite
652 was found on the coupon, opaque and came from clay, and is predominantly used as a building material
653 in the region. Chamosite transparency is translucent to sub-translucent and is a mineral found in the
654 environment with low iron deposition. Chanchangi et al. [11] reported that this mineral could be found
655 in laterite and sometimes loamy soil, and these are also used as building materials in the region.
656 Spodumene is obtained when minerals are ignited, and this could be due removal or breaking of rocks
657 for road construction, quarry activity or mining. These minerals identified from the ABV coupon show
658 that the region's high soiling rate is directly related to construction activity and weather activity. To
659 further validate the minerals recorded, the main pollutant and AQI from Table 2 were analysed, which
660 shows that PM_{10} and $PM_{2.5}$ are very high values; this supports the claim that particles recorded on the
661 coupons are from construction sites, landfills, and windblown dust.

662

663 Findings show optical losses on all coupons, even though few are minor. However, accumulation causes
664 required additional information, as included in some paragraphs above. The analysis shows that
665 particles in the atmosphere or the AQI cannot be used as the only source for determining the
666 accumulation rate as wind speed, humidity, and precipitation could play a vital role in allowing particles
667 settlement on surfaces.

668

669 The soiling mapping result presented in the previous section highlighted a significant variation between
670 the result from this study and information presented by the GSA, with higher soiling rates determined
671 during this study. The variation observed from the annual mapping is significantly wide. The maximum
672 variation was observed from ABV, where a 746.69 kWh/kWp difference was recorded between the PV
673 output using soiling data from this study and the PV yield based on 4.5% soiling. All the annual soiling
674 data from the other sites in this study presented higher soiling losses than the GSA constant value,
675 shown in Fig. 5.

676

677 Each season presented a massive variation between the PV yield (with soiling data obtained from this
678 study) and GSA PV yield (a constant soiling rate of 4.5%). The maps show that the most significant
679 disparity recorded in the Northern region during the dry season was from ABV with about 536.14
680 kWh/kWp difference, while the most significant disparity recorded during the wet season was from
681 PHC with about 388.12 kWh/kWp. This regional soiling disparity that is directly related to seasons is
682 due to the intertropical displacement caused by the Coriolis force. During the dry season, the PV yield
683 is higher in the Northern region, and the most significant soiling loss was recorded in the North-central.
684 While during the wet season, the Southern part tends to have a high PV yield due to the more extended

685 duration of the season in the region and the most significant soiling loss was recorded in the South-
 686 south region. As earlier mentioned, the dust movement is influenced by north-easterly low-level jets
 687 wind from the Saharan desert during the dry season. During the wet season, the dust movement is
 688 influenced by south-westerly winds from the Gulf of Guineas and the Niger-Delta region, where oil
 689 exploration activities are ongoing. By observing the pattern of the weather information provided in Fig.
 690 2 (a) to (g), it is easy to know that the Northern and the Southern region have a climatic pattern that
 691 substantially influences dust settlement and accumulation on an exposed surface. The maps in Fig. 6
 692 and Fig. 7 illustrated higher PV yield degradation due to soiling rates in both seasons compared to GSA
 693 values, and these seasonal variation data can be found in Fig. 8.

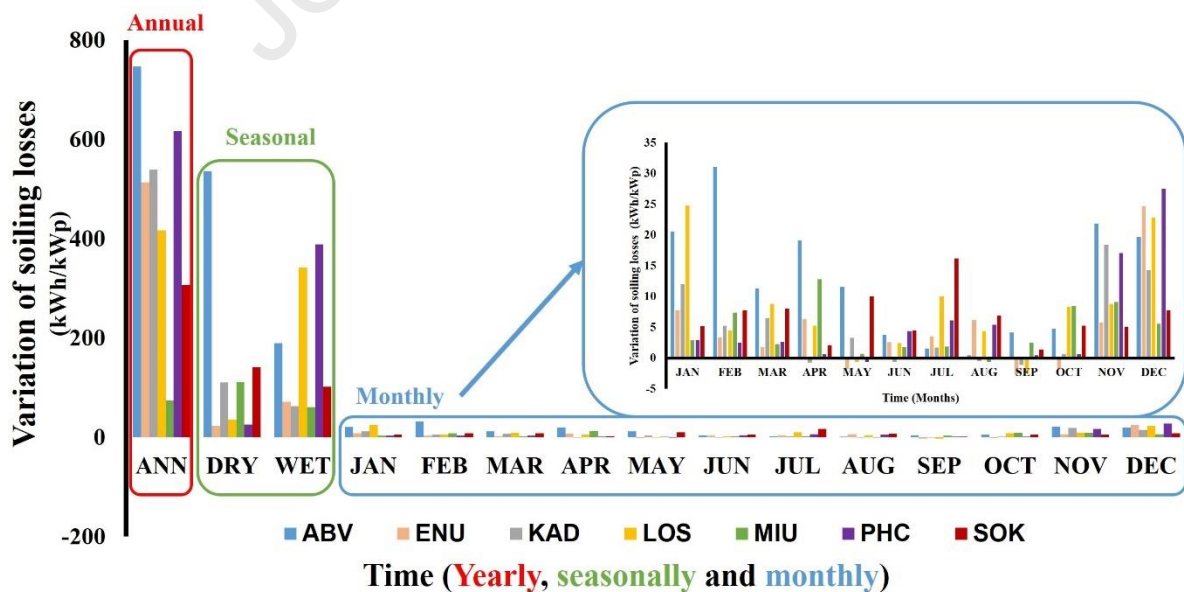
694

695 It is necessary to understand the monthly PV yield, considering the effect of soiling. There are individual
 696 monthly differences between PV yield employing soiling data from this study and PV yield with a 4.5%
 697 constant soiling rate. A closer examination of results reveals that some months (mainly during the dry
 698 season), such as November, December, January, February, March and April, have a higher PV yield
 699 degradation rate variation. The most significant variation was observed in February, where about 31.05
 700 kWh/kWp disparity was recorded in ABV, followed by December with 27.53 kWh/kWp in PHC,
 701 January with 24.81 kWh/kWp in LOS, November with 21.85 kWh/kWp in ABV. The few negative
 702 figures shown in Fig. 8 are when GSA soiling rates in percentage become higher than the optical losses
 703 recorded from this study. Variations are minor during the months that fall within the wet season. Some
 704 months have PV yield with soiling values that turns out to be lower than GSA values because the soiling
 705 loss is lower than 4.5% (GSA soiling loss). The map for the month of May illustrated that PV yield
 706 (with soiling determined from this study) in three regions (ENU, LOS, and PHC), all from the Southern
 707 part of the country are less than 4.5% (GSA soiling loss value); the June map shows only one region
 708 (KAD); the August map shows two areas (KAD and MIU); the September map shows three regions
 709 (ENU, KAD, and LOS); while the October map shows only one region (ENU). Variation data for each
 710 month is shown in Fig. 8.

711

712 As earlier stated, the PV yield presented in the Global solar atlas was clearly emphasised that it does
 713 not adequately account for a number of important factors that potentially impact the PV output.
 714 However, soiling data cannot be constant, and caution should be taken when generalising such
 715 information since it can significantly impact the PV yield and mislead the potential users of the
 716 information. The findings demonstrated more realistic and accurate soiling losses, as shown in Fig. 8,
 717 where the disparity values of the soiling site were illustrated, comparing PV yield with soiling data from
 718 this study and GSA PV yield with constant 4.5% soiling considering the exposure period.

719



720

721 Fig. 8. Variation of soiling losses between GSA and results from this study. The ANN highlights the
 722 annual variation, Dry and Wet show the seasonal variation, highlighting dry seasonal variations and the

723 latter shows wet seasonal variations for the seven regions. The Monthly illustrates the variation of each
724 region in every calendar month. Soiling stations are highlighted using various colours in the chart.
725

726 The low-cost novel approach employed in this study has potential advantages; it could guide research
727 to know the appropriate mitigating techniques required for a particular region in the country and prompt
728 a significant step toward finding a lasting solution to the PV soiling problem. The presented research
729 concept could be replicated elsewhere, from regional to global scale. Furthermore, it could be used for
730 other applications in the glass (to determine the period cleaning cycle for cleaning exposed glass to
731 reduce cost); financial (to calculate more accurate funding to invest in developing large scale solar
732 energy assets); chemical (provide information on the appropriate chemical material to use for
733 developing self-cleaning coating); mechanical (to types of machinery that could be used for optimum
734 maintenance design at lower cost); and mining industries (to highlight potential mineral deposition
735 across the region of study). It is clear that there are significant benefits from the output of this study
736 since the previous information is somehow misleading due to less accuracy of the soiling information,
737 which might be causing wrong installation and maintenance planning that could lead to less yield or
738 system failure at the extremity. The findings provided benefits such as more accurate and realistic
739 information for better PV installation and maintenance planning to achieve more yield. The result could
740 assist in optimising the maintenance procedure to generate more output at less maintenance cost.
741

742 **5 Conclusion**

743 Soiling has a detrimental effect on PV performance, and this problem is unacceptably underestimated
744 and understudied in some regions, such as Nigeria, with massive solar energy potential, low PV
745 penetration and high energy deficit. This study demonstrated high optical losses in a region with
746 enormous solar energy potential but shallow PV penetration. The results show that coupons positioned
747 on horizontal planes accumulate more dust than the tilt angle (45°) and vertical plane, providing a
748 positive advantage of less soiling losses to integrated RE due to varying angular position. The work
749 reveals ABV as the region with the most significant soiling loss in the country and February as the
750 month when the most considerable soiling loss occurs. The outcome shows that the Northern region has
751 a higher soiling loss during the dry season, with ABV having the most significant loss, while during the
752 wet season, the Southern region shows a higher accumulation, with LOS and PHC being on top of the
753 list. SEM/EDX analysis confirmed that minerals collected on coupon surfaces negatively affect light
754 transmittance, causing the optical losses to be recorded. The AQI and pollutant data validate the type
755 of particles recorded. The weather condition shows why high accumulation values are recorded from
756 each region and during a specific season, impacting seasonality variation. The significant disparity has
757 been illustrated when results from this study are correlated with already published work.
758

759 The study demonstrated a unique technique that investigated optical losses by employing a radical
760 approach and showing a wide variation of soiling losses which has been under-reported by previous
761 studies and also grossly underestimated, which might be due to overlooking regional variability and the
762 seasonal difference that plays a vital role in increasing or decreasing the losses rate. In conclusion, this
763 work offers a successful low-cost approach that could be employed to determine soiling induced losses
764 on PV worldwide. However, the method could be further refined by increasing the number of soiling
765 stations and narrowing the distance. It is recommended that a similar soiling station should be installed
766 in some regions to acquire *in-situ* soiling data that would reduce the variation gap discovered in this
767 study and provide researchers, policymakers, potential PV investors, and commercial PV companies
768 with more realistic PV yield potential. Finally, the information presented in this study should use to
769 determine the appropriate cleaning procedure and optimising it to improve the penetration and scale-up
770 of the solar energy technologies in regions with high energy demand and low penetration to achieve the
771 sustainable development target goal 7 [37] ("*Ensure access to affordable, reliable, sustainable and
772 modern energy for all*").
773

774 **Acknowledgement**

775 This study is funded through a PhD research grant to Yusuf N. Chanchangi from the Petroleum
776 Technology Development Fund, with additional support from the 'Joint UK Indian Clean Energy Center
777 (JUICE)' and the RCUK's Energy Program (Contract No: EP/P003605/1). The EPSRC IAA grant
778 (Contract No-EP/R511699/1) obtained from Dr Aritra Ghosh also supported this work. The authors

779 gratefully acknowledge all the funding. All the original materials and data can be accessed upon request
780 via email to the corresponding authors in support of open access research. The study was conducted in
781 collaboration with the Nigerian Civil Aviation Authority, Solar Energy Research Centre Usman Dan
782 Fodio University, Sokoto, National Centre for Energy Research and Development, University of
783 Nigeria Nsukka, and Dornier Aviation Nigeria. The authors gratefully acknowledge the assistance and
784 expertise of all the people involved in this research. This paper's content is solely the authors'
785 responsibility and may not necessarily represent the views of funders and collaborators as both were
786 not directly involved in writing the article.

787

788 Author information**789 Affiliations**

790 **Solar Energy Laboratory, Environment and Sustainability Institute (ESI), University of Exeter,**
791 **Cornwall Campus Penryn, TR10 9FE, United Kingdom**

792 Yusuf N. Chanchangi

793

794 **College of Engineering, Mathematics and Physical Sciences, Environment and Sustainability**
795 **Institute (ESI), University of Exeter, Cornwall Campus Penryn, TR10 9FE, United Kingdom**

796 Aritra Ghosh, Sentilarasu Sundaram, and Tapas, K. Mallick

797

798 **Advances in Photovoltaic Technology (AdPVTech), CEACTEMA, University of Jaén, 23071**
799 **Jaén, Spain**

800 Leonardo Micheli and Eduardo F. Fernández

801

802 Author contributions

803 Yusuf N. Chanchangi, Aritra Ghosh, Sentilarasu Sundaram, and Tapas K. Mallick designed the study.

804 Yusuf N. Chanchangi and Aritra Ghosh conducted the analysis.

805 Yusuf Chanchangi wrote the initial draft.

806 Tapas K. Mallick, Aritra Ghosh, Leonardo Micheli, and Eduardo F. Fernández contributed to
807 methodological refinements and conceptual considerations.

808 All authors contributed to the manuscript's completion through comments and edits of the text and
809 figures.

810

811 Competing interests

812 The authors declare no competing interests.

813

814 Additional information

815 Supplementary Material.

816

817 Correspondence

818 Correspondence and requests for materials should be addressed to Yusuf Nadabo Chanchangi.

819

820 **References**

- 821 [1]. REN21, *Renewables 2020: Global Status Report*. 2020: Paris: REN21 Secretariat.
- 822 [2]. Chanchangi, Y.N., Ghosh, A., Sundaram, S., and Mallick, T. K., *Dust and PV Performance in*
823 *Nigeria: A review*. Renewable and Sustainable Energy Reviews 2020. **121**(2020): p. 1.
- 824 [3]. Gupta, V., Sharma, M., Pachauri, R. K., and Babu, K. N. D., *Comprehensive review on effect*
825 *of dust on solar photovoltaic system and mitigation techniques*. Solar Energy, 2019. **191**(2019):
826 p. 596-622.
- 827 [4]. Costa, S.C.S., Sonia, A., Diniz, A. C. and Kazmerski, L. L., *Solar energy dust and soiling R&D*
828 *progress: Literature review update for 2016*. Renewable and Sustainable Energy Reviews
829 2018. **82** (2018): p. 2504-2536.
- 830 [5]. Zaihidee, F.M., Mekhilef, S., Seyed, M., and Horan, B., *Dust as an unalterable deteriorative*
831 *factor affecting PV panel's efficiency: Why and how*. Renewable and Sustainable Energy
832 Review, 2016. **65**(2016): p. 1267-1278.
- 833 [6]. Cano, J., John, J. J., Tatapudil, S. and TamizhManil, G., *Effect of Tilt Angle on Soiling of*
834 *Photovoltaic Modules*, in *2014 IEEE 40th Photovoltaic Specialist Conference (PVSC)*. 2014,
835 IEEE: Denver, CO USA. p. 3174-3176.
- 836 [7]. Ghazi, S., and Ip, K., *The effect of weather conditions on the efficiency of PV panels in the*
837 *southeast of UK*. Renewable Energy, 2014. **69** (2014): p. 50-59.
- 838 [8]. Sulaiman, S.A., Guangul, F. M., Hidayat-Mat., M. N., and Mohammed Bou-Rabee, A., *Real-*
839 *Time Study on the Effect of Dust Accumulation on Performance of Solar PV Panels in Malaysia*
840 *in 1 st International Conference on Electrical and Information Technologies ICEIT'2015*. 2015,
841 IEEE: March 25-27, 2015 Marrakech, Morocco.
- 842 [9]. Alnaser, N.W., Al Othman, M. J., Dakhel, A. A., Batarseh, I., Lee, J.K., Najmaii, S.,
843 Alothman, A., Al Shawaikh, H. and Alnaser, W.E., *Comparison between performance of man-*
844 *made and naturally cleaned PV panels in a middle of a desert*. Renewable and Sustainable
845 Energy Reviews, 2018. **82** (2018): p. 1048-1055.
- 846 [10]. Adinoyi, M.J., and Said, S. A. M., *Effect of dust accumulation on the power outputs of solar*
847 *photovoltaic modules*. Renewable Energy 2013. **60** (2013): p. 633-636.
- 848 [11]. Chanchangi, Y.N., Ghosh, A., Sundaram, S. and Mallick, T. K., *An analytical indoor*
849 *experimental study on the effect of soiling on PV, focusing on dust properties and PV surface*
850 *material*. Solar Energy, 2020. **203** (2020): p. 46–68.
- 851 [12]. Australian-Standard, *AS 4509.2-2002 Stand-alone power systems - System design guidelines*,
852 *in 3.4.3.6 Derating Factor*. 2002, Standards Australia International Ltd: Sydney, Australia.
- 853 [13]. Patrick, D.B., and Bruce, H. K., *A Handbook on Artificial Soils for Indoor Photovoltaic Soiling*
854 *Tests*, in *SAND2014-19199*. 2014, Sandia National Laboratories, Sandia Corporation:
855 Albuquerque.
- 856 [14]. Enphase-Energy, *Guide to PVWatts Derate Factors for Enphase Systems When Using PV*
857 *System Design Tools*. 2014, Enphase Energy: Online.
- 858 [15]. Tanesab, J., Parlevliet, D., Whale, J. and Urmee, T., *Energy and economic losses caused by*
859 *dust on residential photovoltaic (PV) systems deployed in different climate areas*. Renewable
860 Energy 2018. **120** (2018): p. 401-412.
- 861 [16]. GSA. *Site*. 2021 [cited 2021 01/02/2021]; Available from:
862 <https://globalsolaratlas.info/map?c=11.894839,8.536414,11&s=11.894839,8.536414&m=site>
- 863 [17]. Li, X., Mauzerall, D. L., and Bergin, M. H., *Global reduction of solar power generation*
864 *efficiency due to aerosols and panel soiling*. Nature Sustainability, 2020. **3**(2020): p. 720–727.
- 865 [18]. Mekhilef, S., Saidur, R. and Kamalisarvestani, M., *Effect of dust, humidity and air velocity on*
866 *efficiency of photovoltaic cells*. Renewable and Sustainable Energy Reviews 2012. **16** (2012):
867 p. 2920- 2925.
- 868 [19]. Saidan, M., et al., *Experimental study on the effect of dust deposition on solar photovoltaic*
869 *panels in desert environment*. Renewable Energy, 2016. **92**: p. 499-505.
- 870 [20]. Chanchangi, Y.N., et al., *Soiling on PV performance influenced by weather parameters in*
871 *Northern Nigeria*. Renewable Energy, 2021.
- 872 [21]. Chanchangi, Y.N., et al., *In-situ assessment of photovoltaic soiling mitigation techniques in*
873 *northern Nigeria*. Energy Conversion and Management, 2021. **244**: p. 114442.
- 874 [22]. Mithhu, M.H., Rima, T. A., and Khan, M. R., *Global analysis of optimal cleaning cycle and*
875 *profit of soiling affected solar panels*. Applied Energy, 2021. **285**(2021): p. 1-10.

- 876 [23]. Micheli, L., Deceglie, M. G., and Muller, M., *Mapping Photovoltaic Soiling Using Spatial*
877 *Interpolation Techniques*. IEEE Journal of photovoltaics, 2019. **9**(1): p. 272-277.
- 878 [24]. Cordero, R.R., Damiani, A., Laroze, D., MacDonell, S., Jorquera, J., Sepúlveda, E., Feron, S.,
879 Llanillo, P., Labbe, F., Carrasco, J., Ferrer, J., and Torres, G., *Effects of soiling on photovoltaic*
880 *(PV) modules in the Atacama Desert*. Scientific Reports, 2018. **8**(13943): p. 1-14.
- 881 [25]. Said, S.A.M., and Walwil, H. M., *Fundamental studies on dust fouling effects on PV module*
882 *performance*. Solar Energy, 2014. **107**(2014): p. 328-337.
- 883 [26]. Mani, M., and Pillai, R., *Impact of dust on solar photovoltaic (PV) performance: Research*
884 *status, challenges and recommendations*. Renewable and Sustainable Energy Reviews 2010.
885 **14** (2010): p. 3124-3131.
- 886 [27]. Tanaka, T.Y., and Chiba, C., *A numerical study of the contributions of dust source regions to*
887 *the global dust budget*. Global and Planetary Change 2006. **52** (2006): p. 88-104.
- 888 [28]. World-Bank. *Indicator*. 2021 2021 [cited 2021 24/02/2021]; Available from:
889 <https://data.worldbank.org/indicator/SP.POP.TOTL?locations=NG>.
- 890 [29]. IEA. *Nigeria_Energy_Outlook: Analysis from Africa Energy Outlook 2019*. 2021 8 November
891 2019 [cited 2021 20/02/2021]; Available from: [https://www.iea.org/articles/nigeria-energy-](https://www.iea.org/articles/nigeria-energy-outlook)
892 [outlook](https://www.iea.org/articles/nigeria-energy-outlook)
- 893 [30]. Coello, M. and L. Boyle, *Simple Model for Predicting Time Series Soiling of Photovoltaic*
894 *Panels*. IEEE Journal of Photovoltaics, 2019. **9**(5): p. 1382-1387.
- 895 [31]. Javed, W., Guo, B. and Figgis, B., *Modeling of photovoltaic soiling loss as a function of*
896 *environmental variables*. Solar Energy, 2017. **157** (2017): p. 397-407.
- 897 [32]. World-Weather-Online. *Weather*. 2019 [cited 2019 14/11/2019]; Available from:
898 <https://www.worldweatheronline.com/>.
- 899 [33]. Air-Plume-Labs. *Air Quality Index*. 2020 [cited 2020 14/11/2020]; Available from:
900 <https://air.plumelabs.com/en/>.
- 901 [34]. Venkatramanan, S., Chung, S. Y., and Prasanna, M. V., *GIS and Geostatistical Techniques for*
902 *Groundwater Science*. 2019, Amsterdam, Netherlands: Elsevier.
- 903 [35]. CCE-NEWS-TEAM. *5 largest construction companies in Abuja, Nigeria*. [Online] 2020
904 12/July/2020 [cited 2020 25/11/2020]; Available from:
905 <https://cceonlinenews.com/2020/07/12/5-largest-construction-companies-in-abuja-nigeria/>.
- 906 [36]. Gholami, A., Saboonchi, A. and Alemrajabi, A. A., *Experimental study of factors affecting dust*
907 *accumulation and their effects on the transmission coefficient of glass for solar applications*.
908 Renewable Energy 2017. **112** (2017): p. 466-473.
- 909 [37]. SDGs-UN. *Goal 7*. 2021 [cited 2021 09/05/2021]; Available from:
910 <https://sdgs.un.org/goals/goal7>.
- 911

Author contributions

Yusuf N. Chanchangi, Aritra Ghosh, Sentilarasu Sundaram, and Tapas K. Mallick designed the study.

Yusuf N. Chanchangi and Aritra Ghosh conducted the analysis.

Yusuf Chanchangi wrote the initial draft.

Tapas K. Mallick, Aritra Ghosh, Leonardo Micheli, and Eduardo F. Fernández contributed to methodological refinements and conceptual considerations.

All authors contributed to the completion of the manuscript through comments and edits of the text and figures.

Journal Pre-proof

Competing interests

The authors declare no competing interests.

Journal Pre-proof